Primary ore Cu mineralization at the Ľubietová-Podlipa locality (Slovakia)

Jarmila Luptáková[1], Stanislava Milovská[1], Stanislav Jeleň[1,2], Tomáš Mikuš[1], Rastislav Milovský[1] & Adrian Biroň[1]

[1]Earth Science Institute, Slovak Academy of Sciences, Ďumbierska 1, 974 11 Banská Bystrica, Slovakia; luptak@savbb.sk, milovska@savbb.sk, jelen@savbb.sk, mikus@savbb.sk, milovsky@savbb.sk, biron@savbb.sk
[2]Department of Geography and Geology, Faculty of Natural Sciences, Matej Bel University, Tajovského 40, 974 01 Banská Bystrica, Slovakia

AGEOS

Primárna rudná Cu mineralizácia na lokalite Ľubietová-Podlipa (Slovensko)

Abstract: The results of mineralogical and geochemical research of primary mineralization at the Ľubietová-Podlipa deposit dumps are presented in the article. Chalcopyrite and tennantite are the most abundant sulphides in studied samples. Cobaltite-gersdorffite, pyrite, siegenite, and cassiterite are quite common, yet volumetrically negligible, in contrast to tetrahedrite, kupčíkite, matildite(?), cinnabar, unidentified Ag-S and native gold, which are very scarce. Gangue minerals are quartz (probably two generations) with fewer amounts of carbonates. Dark quartz is often hosting irregular nests of sulphide minerals, usually on outer boundaries of the veins. Both generations of vein quartz show similar microstructures of low-temperature ductile deformation. Carbonates include members of dolomite-ankerite series, siderite, and calcite containing variable amounts of Fe and Mn. Isotopic composition of $\delta_{34}S$ in chalcopyrite and tennantite vary between 6.69 and 9.77 ‰. These values may be very close to the composition of H_2S in fluid, which is tentatively attributed to a deep source derived from metamorphic rocks. Influence of compositional variability of tetrahedrite-tennantite series and carbonates on Raman shift of selected vibration bands is also a subject of this study.

Key words: Ľubietová - Podlipa, Cu-mineralization, cobaltite, gersdorffite, kupčíkite, carbonates

1. INTRODUCTION

The small region around the municipality of Ľubietová has a rich mining history that dates back to the 14st century (Vlachovič, 1964). There were three small deposits near Ľubietová called Podlipa, Svätodušná, and Kolba. Bergfest (1951) reported that the ore veins in Podlipa yielded 25,000 tons of copper and 1,750 tons of silver in course of about 500 years (Bergfest, 1951). Ore exploitation in the past targeted exclusively the unusually well developed oxidation and cementation zones of the ore bodies.

Extensive dumps as well as some accessible parts of the old mines are regularly subject of interest of scientists and mineral collectors. Podlipa is the type locality of libethenite (Breihaupt, 1823) and mrázekite (Řídkošil et al., 1992) and hosts also other rare minerals such as ludjibaite and reichenbachite (Hyršl, 1991). Current scientific effort focuses on comprehensive assessment of all available geological, geochemical, and mineralogical data with the aim of remediation of the environmental pollution at the site.

In the past years, we have been studying weathering processes, element distribution and migration of elements at the Podlipa site (Luptáková et al., 2012; Milovská et al., 2014). The primary mineralogy, however, is not known well and was never described in detail. Since the primary minerals are a significant component of the geochemical environment around the deposit and could be a source of the pollution, their identification and description is a necessary step in such projects. This work provides a detailed description of the primary minerals found on the old dumps of the Podlipa deposits. Using a combination of optical microscopy, powder X-ray diffraction, electron microprobe, and Raman spectroscopy, we have identified all primary minerals at the Podlipa. In addition, the work brings new data on sulphur isotopic composition of primary sulphides from the Podlipa.

2. GEOLOGICAL SETTING

The Podlipa ore deposit is situated in Veporské vrchy Mts. (central Slovakia), about 1 km east of Ľubietová village on the southern slope of Vysoká Mt. (995.5 m) above the Zelená dolina valley. The rich history of mining, ore processing and mineralogical composition of the ores attracted also the attention of many geoscientists who investigated petrology, regional geology, and tectonics (Vozárová & Vozár, 1988; Polák et al., 2003), economic geology (Kravjanský, 1956; Hauerová et al., 1989) and mineralogy (Láznička, 1966; Figuschová, 1977; Řídkošil & Povondra, 1982; Hyršl J., 1991; Řídkošil et al., 1992; Andráš et al., 2009; Michňová et al., 2008; Michňová, 2009; Luptáková et al., 2012). The Podlipa deposit and its surrounding is hosted by several contrasting lithologies (Fig. 1). The pre-Quaternary geological structure is composed of the Veporic Superunit, discordantly overlain by Neogene volcanic rocks. The Veporic Superunit comprises a steeply inclined NW plunging stack of metamorphosed rocks, involving from SE to NW: migmatised ortho- and paragneisses of unknown Palaeozoic age, Permian volcano-sedimentary sequence of metasandstones and arkoses with acidic to intermediate effusives, Induan quartzites and sandstones, Olenekian lagoonal variegated shales, sandstones, and carbonates, Middle Triassic dolostones. Upper Miocene volcanic rocks of the Poľana

Manuscript received: 2016-09-12
Revised version accepted: 2016-12-13

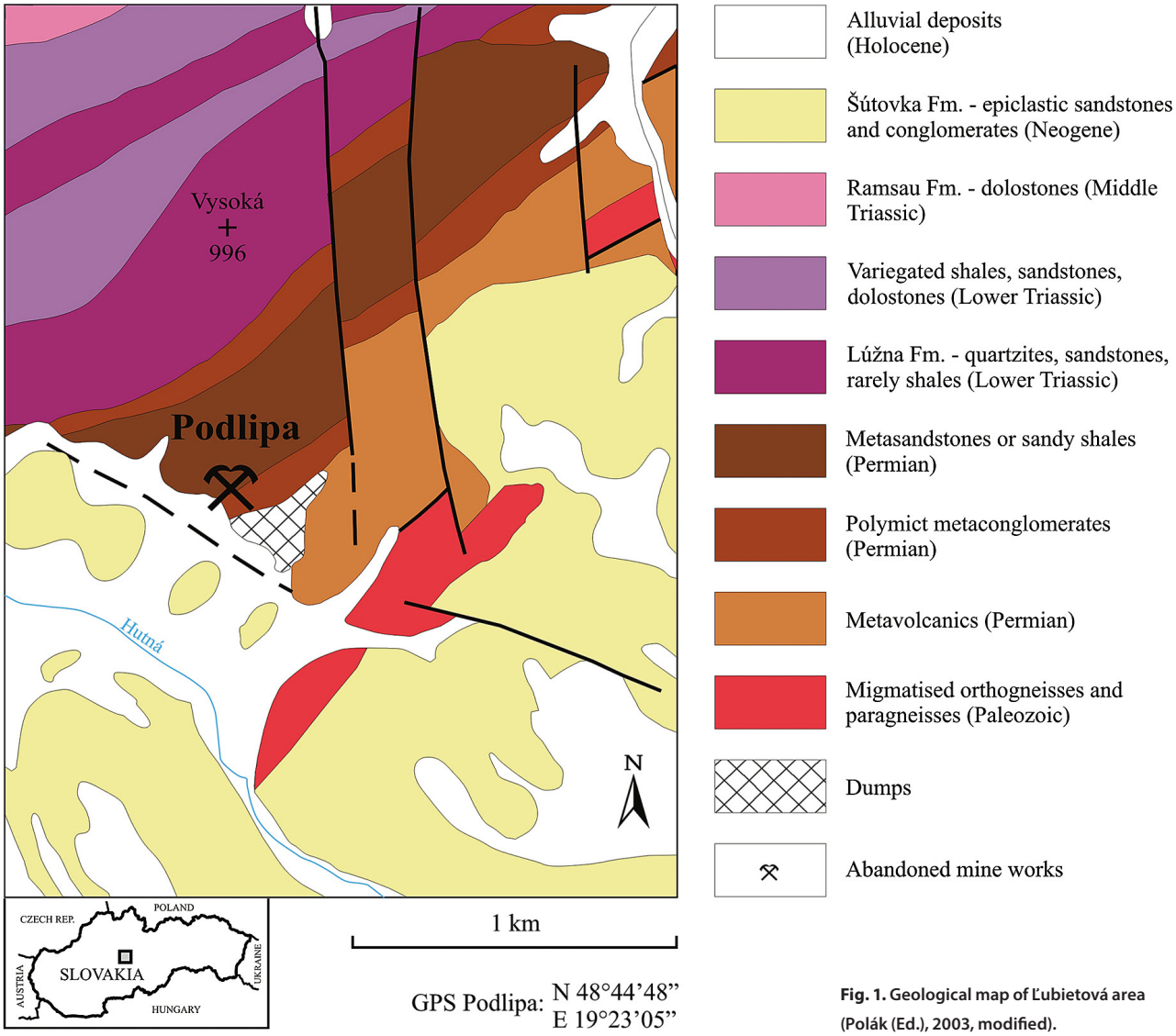

Fig. 1. Geological map of Ľubietová area (Polák (Ed.), 2003, modified).

Stratovolcano are andesitic epiclastic sandstones and conglomerates. Copper mineralization is emplaced mainly in feldspar-rich Permian metasandstones and greywackes, as well as in the underlying orthogneisses. Epigenetic hydrothermal vein, stockwork, and sporadically stockwork-impregnation mineralization forms veins, lenses, and nests emplaced in the E–W or N–S trending tectonized zones, cutting discordantly the lithologies of the Veporic Superunit (Slavkay et al., 2004). Ore bodies have a typical length of several hundred meters. Vein texture is massive and brecciated (Hauerová et al., 1989; Koděra (Ed.), 1990; Zuberec et al., 2005). There is a stockwork zone in the southern part of the deposit, impregnation ores can be also locally found. The ore veins are enveloped by halos of hydrothermal alteration, especially silicification and sericitization. Wallrocks of the deposit are often deformed by brittle shear zones or faults. Mineralization was formed during the Cretaceous Palaeo-Alpine stage of Western Carpathian tectonic evolution on a system of transtensional shear zones with transitions to extensional faults (Lexa et al., 2007). According to Hauerová et al. (1989), the mineralization at the Ľubietová-Podlipa deposit developed in two mineralization stages – carbonate and sulphide. The deposit was exploited by underground mining in about 21 adits and shafts in an altitude range of 570 to 700 m a.s.l. (Fig. 2).

3. MATERIALS AND METHODS

All the studied samples were collected at mine dumps of the Podlipa deposit. Their localization is indicated in Fig. 2.

3.1. Scanning electron microscopy with energy-dispersive X-ray spectroscopy (SEM-EDS)

Scanning electron microscope JEOL JSM-6390LV (Earth Science Institute, SAS, Banská Bystrica) coupled with energy-dispersive X-ray detector (EDS, Oxford Instruments INCA x-act) was used for imaging of textures in ore veins and rocks in backscattered electrons, and for acquisition of semi-quantitative elemental analyses in polished section and thin section samples.

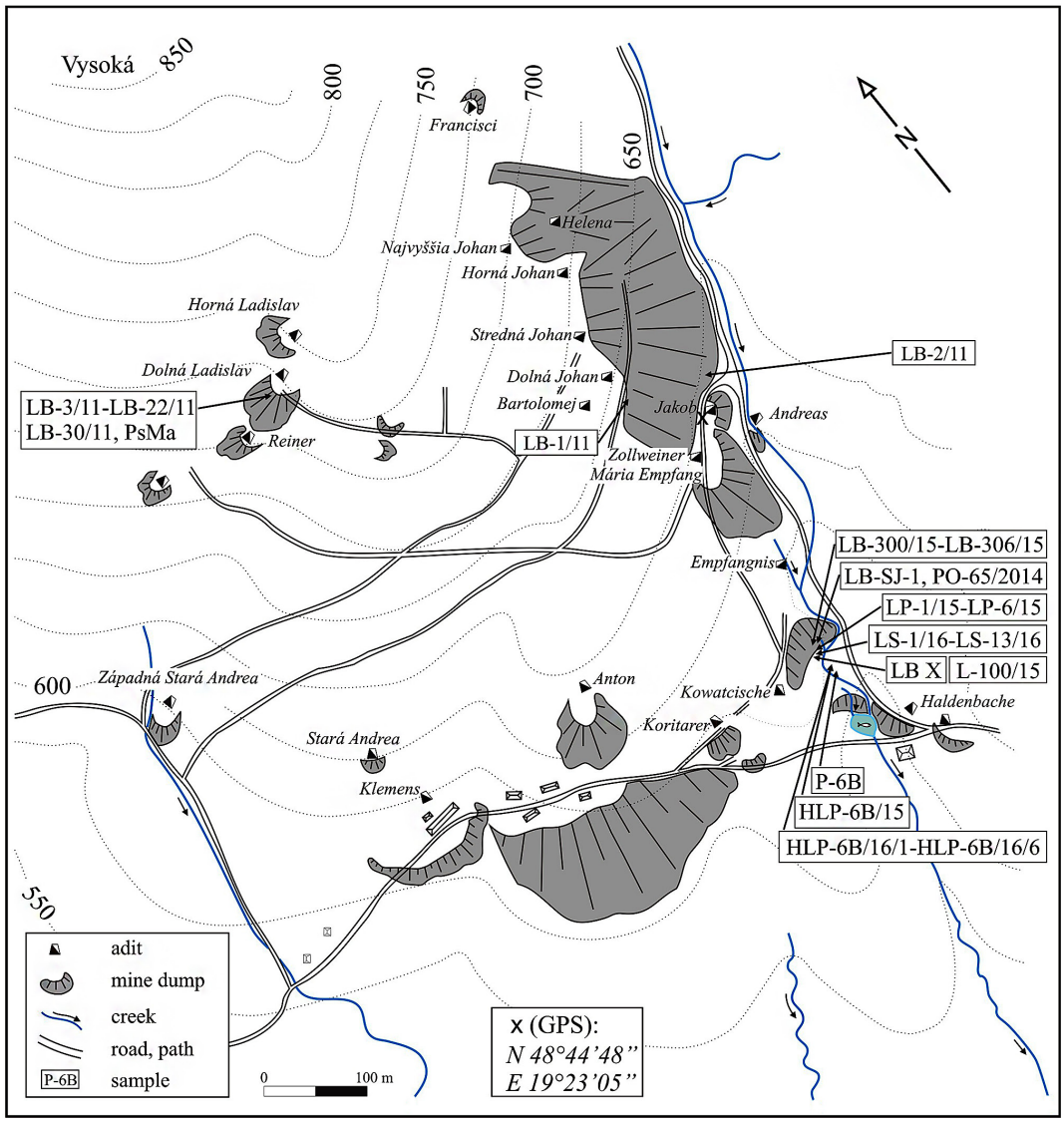

Fig. 2. Situation of the old mining works at the Podlipa deposit in Ľubietová (modified after Ilavský et al., 1978) with localization of samples.

Qualitative analyses of minerals were made under following conditions: acc. voltage 15 kV, WD 10 mm, probe current 15 nA, beam diameter 1 μm.

3.2. Wavelength-dispersive spectrometry (WDS)

Ore minerals – sulphides, sulphosalts, arsenides, carbonates, cassiterite, and gold – were studied in course of years 2011–2016 using wavelength-dispersive spectrometry (WDS) on two electron probe microanalyzers (EPMA) at following conditions:

1) instrument CAMECA SX-100 (State Geological Institute of D. Štúr in Bratislava) – accelerating voltage 25 kV, probe current 10 nA, beam diameter 3–5 μm and ZAF correction. Used standards, analyzed lines and counting time were as follows: pure Ag (Ag Lα, 10 s), pure Cd (Cd Lα, 10 s), $CuFeS_2$ (S Kα, 10 s), PbS (Pb Mα, 10 s), pure Bi (Bi Lα, 60 s), pure Co (Co Kα, 10 s), HgS (Hg Lα, 100 s), pure Ni (Ni Kα, 10 s), InSb (Sb Lβ, 90 s), GaAs (As Lα, 10 for chalcopyrite, 60 for sulphoarsenides), pure Cu (Cu Kα, 10 s), FeS_2 (Fe Kα, 10 s), Bi_2Se_3 (Se Lα, 60 s) and ZnS (Zn Kα, 10 s). Conditions for cassiterite: accelerating voltage 20 kV, probe current 20 nA, beam diameter 2 μm, ZAF correction, counting time 10 s on peak. Used standards and lines: Sn(Lα) – SnO_2, Ti(Kα) – TiO_2, V(Kα) – V, Fe(Kα) – fayalite, Mg(Kα) – MgO, Ca(Kα) – wollastonite, W(Lα) – W.

2) instrument JEOL JXA 8530FE (Earth Sciences Institute in Banská Bystrica) at following conditions: accelerating voltage 20 kV, probe current 15 and 20 nA, beam diameter 2–3 μm, ZAF correction, counting time 20 s on peak, 10 s on background. Used standards, X-ray lines and D.L. (in ppm) are: Au (Mα, 162) – pure Au, Ag(Lα, 45) – pure Ag, S(Kα, 26) – pyrite, Cu(Kα, 39) and Fe(Kα, 26) – chalcopyrite, As(Lβ, 208) – GaAs, Se(Lβ, 281) – Bi_2Se_3, Cd(Lα, 55) – CdTe, Sb(Lα, 47) – stibnite, Hg(Mα, 101) – cinnabar, Bi(Lα, 240) – Bi_2S_3, Pb(Mα, 93) – galena, Ni(Kα, 32) – gersdorffite, Co(Kα, 32) – pure Co, Zn (Kα, 45) – sphalerite. Carbonates: accelerating voltage 15 kV, probe current 10 nA, beam diameter 8 μm, counting time 10 s on peak, 5 s on background. Standards: Ca(Kα, 25) – diopside, Ba(Mα, 105) – barite, Mn(Kα, 70) – rodonite, Mg(Kα, 27) – olivine, Si(Kα, 74) – plagioclase, Sr(Kα, 112) – celestine, Fe(Kα, 89) – hematite, Cu(Kα, 112) – cuprite, Zn(Kα, 150) – willemite.

3.3. Raman microspectroscopy

Raman microspectroscopy was used for the characterization of tennantite, tetrahedrite, and carbonates. Minerals were studied in polished and thin sections as well as on broken rock surfaces. Raman spectra were acquired at room temperature with a LabRAM *HR* (Horiba Jobin-Yvon) microspectrometer (Earth Sciences Institute in Banská Bystrica), based on an Olympus BX41 microscope with confocally coupled Czerny-Turner type monochromator (focal length 800 mm). A laser emission at λ=532 nm was used for excitation, possible artifacts and photoluminescence peaks were excluded after comparison with spectra excited at λ=633 nm. The Raman-scattered light was collected at 180° geometry through a 100× objective lens with numerical aperture 0.8 and dispersed by a diffraction grating with density 600 gr·mm^{-1} onto a cooled CCD detector. The grating turret accuracy was calibrated between zero-order line (180° reflection) and laser line at 0 cm^{-1}. Spectral accuracy was verified on ν_1 peak of silicon which was always within three detector pixels around the theoretical value (520.7 cm^{-1}). Beam intensity was attenuated using neutral density filters, typical power on sample surface was less than 2.4 mW. Eventual thermal damage or spectral effects were excluded by *(i)* visual inspection of excited surface after experiment; *(ii)* observation of possible decay of spectral features in sequence of fast shots at the start of excitation; and *(iii)* checking for thermal downshift of Raman lines. Exposition time was 180 s (4 × 45 s) for carbonates and 2 × 600 s for tetrahedrite/tennantite. The spectra were acquired in the range of 60–2000 cm^{-1}. Positions of Raman lines of carbonates were refined by peak fitting using Gaussian-Lorentzian function in program LabSpec5 (Horiba – Jobin Yvon).

3.4. X-ray powder diffraction analysis

X-ray powder diffraction analysis was employed to identify carbonate minerals. Analyses were performed on a Bruker D8 Advance diffractometer (Earth Sciences Institute in Banská Bystrica) using CuKα radiation generated at 40 kV and 40 mA and Sol-X SDD detector. The beam was collimated with a slit assembly 0.3°–6 mm – 0.3°–0.2 mm, primary and secondary Soller slits. Back-loaded samples were scanned in reflection mode from 2–65° 2Θ with step size 0.02° 2Θ and 1.25 seconds counting time. Experimental data were compared with the PDF2 database.

3.5. Stable isotopes of sulphur

Stable sulphur isotopes were analysed in chalcopyrite and tennantite. Pure mineral grains were hand-picked, powdered in agate mortar and amount of 170 to 400 micrograms of pulver was mixed with equal amount of V_2O_5 and packed into tin capsules. The combustion reactor of an elemental analyser (Flash 2000 HTPlus device, Thermo Scientific) was used for decomposition of samples in stream of oxygen at 1000 °C and further oxidation and reduction of sulphur oxides on WO_3 and electrolytic copper. The purified SO_2 was transferred through a continuous-flow interface into an ion source of the mass spectrometer (MAT253, Thermo Scientific, Earth Sciences Institute in Banská Bystrica). Abundances of isotopes ^{34}S and ^{32}S were calculated from intensities of masses 64, 65, and 66 in samples relative to the reference SO_2 gas. Series of samples were bracketed by calibration standards (international reference materials IAEA-SO6, IAEA-S2, IAEA-S3, and NBS-127) that were used to recalculate the measured isotope values to per mil vs. CDT. Typical external standard deviation for $\delta^{34}S$ values is between 0.14 and 0.23 ‰.

4. RESULTS

4.1. Vein textures

The sulphide-bearing quartz veins are sometimes straight but often of amoeba shape, with thin shoots in random direction, resembling hydraulic opening of fissures. Quartz growth is following druse law with crystal axes directed perpendicular to vein walls and blocky crystals in centres of the veins, which points to crystallization into open space. The middle zone is often hosting carbonate relics or their leached cavities. This texture is further veined by a younger generation of dark quartz, forming filliform network of veinlets in older milky quartz and thicker widely-spaced veins cutting the carbonates

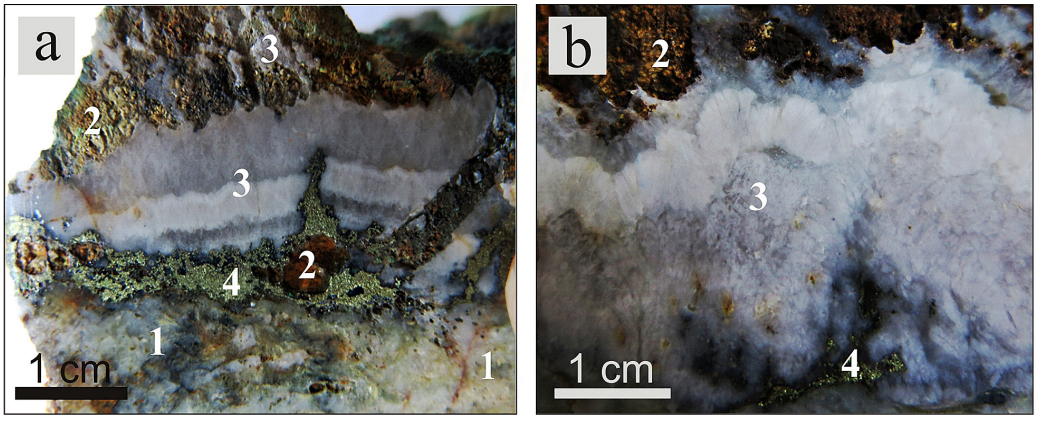

Fig. 3a,b. Vein texture of carbonate-quartz-sulphides association: host silicified metasandstone (1), brecciated and leached carbonate veinlets (2) penetrated by quartz (3), and younger veinlet of sulphides with prevailling chalcopyrite and dark quartz (4) cutting quartz and enclosing carbonate fragments.

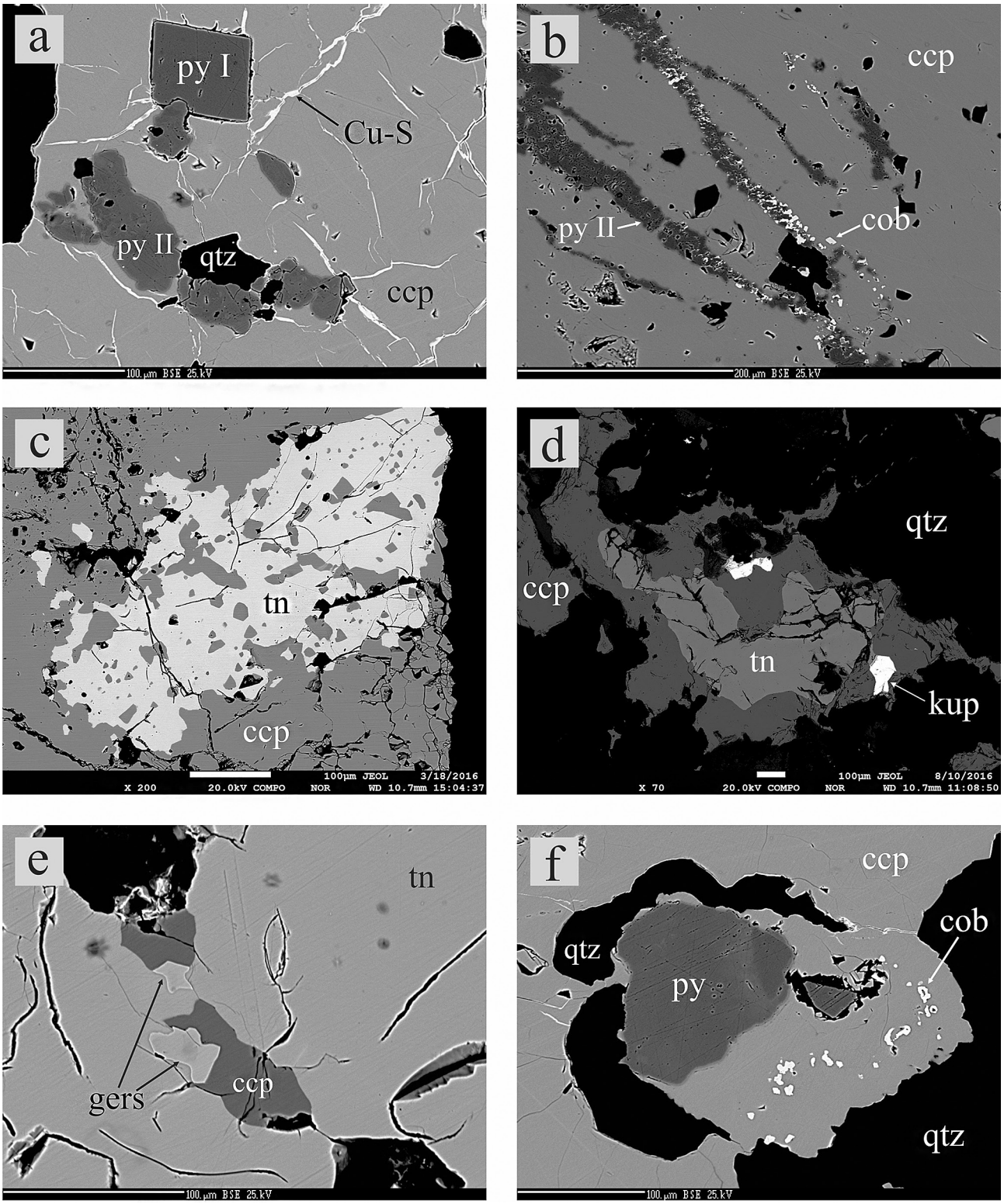

Fig. 4. a) Euhedral pyrite (py I) with irregular pyrite (py II) grains and quartz (qtz) in chalcopyrite (ccp). Thin bright veinlets of the Cu-S phases intersect massive chalcopyrite (ccp); **b)** pyrite (py II) veinlets with impregnations of cobaltite (cob) intersect massive chalcopyrite (ccp); **c)** a tennantite (tn) graphic intergrowth with chalcopyrite (ccp); **d)** aggregate of chalcopyrite (ccp), tennantite (tn) and kupčíkite (kup) in quartz (qtz); **e)** aggregate of small irregular grains of chalcopyrite (ccp) and gersdorffite (gers) in tennantite (tn); **f)** pyrite (py) intergrowths with chalcopyrite (ccp) and quartz (qtz), and cobaltite forming impregnations in chalcopyrite. (BSE)

and forming boxwork textures. This generation of younger, dark quartz hosts often irregular nests of chalcopyrite, usually on outer boundaries of the veins (Fig. 3a,b).

Both generations of vein quartz show similar microstructures of low-temperature ductile deformation as quartz clasts inside rock matrix: lattice bending (undulosity), passing into

Tab. 1. Representative microprobe analyses of chalcopyrite from the Podlipa deposit samples (bdl - below the detection limit).

Mineral	chalcopyrite				
Analysis	1.	2.	3.	4.	5.
Number	LP-1/15	L-100/15	P-6B/15	PO-65/14A	LBSJ-1
			wt. %		
Cu	34.42	34.11	33.93	34.75	34.30
Fe	30.86	30.43	29.61	30.75	29.70
Ag	0.04	0.03	bdl	0.04	0.01
Pb	0.21	0.18	bdl	0.20	0.19
Zn	bdl	bdl	bdl	bdl	bdl
As	0.09	0.08	0.03	0.00	0.00
S	34.76	34.95	35.25	34.55	35.11
Co	0.03	0.00	0.04	0.01	-
Ni	bdl	bdl	bdl	bdl	bdl
Sb	bdl	bdl	bdl	bdl	bdl
Bi	0.00	0.02	0.91	0.00	0.00
Au	bdl	bdl	bdl	bdl	bdl
Cd	-	-	0.02	-	0.03
Hg	-	-	0.00	-	0.00
Se	-	-	0.01	-	-
Sn	-	-	0.01	-	-
Total	100.40	99.80	99.80	100.29	99.34

subgrain rotation and nucleation of tiny new grains, forming bands of equant mosaic in zones of increased strain. No higher-temperature phenomena such as grain-boundary migration or annealing were observed. Carbonates behaved more brittle than quartz; they are commonly twinned and only slightly undulose. Their contrasting rheology is underlined by fracturing of carbonate in more ductile quartz. Weak grade of deformation in veins does not necessarily apply for bulk rock, as the strain was mainly accommodated in its interconnected phyllosilicate matrix, leaving quartz clasts and veins more-or-less passive.

4.2. Minerals

Chalcopyrite is the most abundant sulphide mineral in the studied samples (Fig. 4a–f). Massive aggregates are common (Fig. 4a,b), they usually form rims of quartz-carbonate veins or penetrate into the crushed matrix of the rock. Impregnations of chalcopyrite in rocks are also common. The sulphidic veinlets rarely intersect quartz veins. Chalcopyrite forms intergrowths with tennantite (Fig. 4c) and together they fill cracks and intergranular spaces in dolomite. Chalcopyrite encloses accessory cassiterite, accompanies cobaltite-gersdorffite in small aggregates enclosed in tennantite (Fig. 4e), and rarely forms intergrowths with tetrahedrite and kupčíkite in quartz. Chalcopyrite is usually enriched in Pb (with highest content 0.23 wt. %), Ag (up to 0.04 wt. %) (Tab. 1) and when intergrown with cobaltite-gersdorffite also in Co (up to 0.45 wt. %). Some samples contain Bi (up to 0.91 wt. %), Co (up to 0.04 wt. %), As (up to 0.18 wt. %), and traces of Se, Cd, and Sn. Other elements (Zn, Ni, Sb, Au) were below the detection limit. In samples from cementation and oxidation zone, chalcopyrite aggregates are cut by thin cracks filled by Cu-S sulphides (Fig. 4a). Surface of weathered chalcopyrite is often coated by Cu-S minerals or Fe oxyhydroxides.

Tennantite is the second most common ore mineral, though much less abundant than chalcopyrite. Both minerals are closely associated and often intergrown. Graphic texture was observed in one case (Fig. 4c), but more often tennantite occurs at the rims of the chalcopyrite aggregates or is enclosed in chalcopyrite. In crushed aggregates, there are more cracks in tennantite, implying that this mineral is either older or more brittle than chalcopyrite. Large tennantite aggregates systematically contain tiny inclusions (up to 50 μm) of cobaltite-gersdorffite and chalcopyrite (Fig. 4e). In the BSE image, tennantite appears to be homogenous (Fig. 4e). Simplified formula of tennantite after Moëlo et al. (2008) can be written as $Cu_6[Cu_4(Fe, Zn)_2]As_4S_{13}$. In our samples (Tab. 2), the content of Cu varies between 9.97 and 10.69 apfu, suggesting that part of Cu is presented in a divalent form. Content of Ag is low (0–0.04 apfu). From the divalent metals, Fe (1.13-1.90 apfu) prevails over Zn (0.02-0.31 apfu). Content of other divalent cations is below detection limit or reaches maximally 0.03 apfu. Substitution of trivalent cations is illustrated in Fig. 6. The As content varies from 2.63 to 3.81 apfu, Sb from 0.14 to 1.10 apfu and Bi from 0 to 0.40 apfu (Tab. 2). Composition of tennantite in one sample (PO-65/14) is different (Tab. 2). The amount of Sb (6.03 at. %) almost matches that of As (6.58 at. %) and Zn (5.38 at. %) prevails over Fe (1.87 at. %), and Cu is probably present only in monovalent form. No apparent correlation between Ag/Cu and Fe/Zn is visible in tennantites due to low content of Ag and Zn (Fig. 6). Tennantite is usually replaced by secondary minerals (covellite, pharmacosiderite).

On the contrary, **tetrahedrite** is rare in studied samples (Fig. 5b). It was observed only under the electron microscope and WDS in the form of minute grains (up to 10 μm) in association with chalcopyrite and kupčíkite or chalcopyrite, galena and siegenite or with tennantite. Chemical composition of these grains reflects the mineral association. Tetrahedrite with kupčíkite contains more than 7 wt. % of Bi (0.57 apfu) (Tab. 2). Analysis of tetrahedrite intergrown with siegenite shows 2.21 wt. % of Ni and 1.79 wt. % of Co. (Tab. 2). This is considered to be a contamination from the surrounding minerals.

There are at least two generations of **pyrite** in this deposit. Pyrite I occurs as relatively large (200 μm) euhedral crystals enclosed in chalcopyrite or quartz (Fig. 4a). Euhedral crystals have sometimes pseudorhombic form. Pyrite II occurs in paragenetic association with cobaltite-gersdorffite in the form of small irregularly shaped crystals arranged into chain like clusters in chalcopyrite (Fig. 4b). Contact between pyrite II and chalcopyrite is diffusive. Larger anhedral grains have sometimes weak zoning (Figs. 4f, 5a) that is caused by variations in As content. These pyrite crystals have varying content of As (up to 3.5 wt. %), Co (up to 4.9 wt. %) and Ni (up to 2.5 wt. %) (Tab. 3, Fig. 7). Irregular pyrite grains were also found in quartz. They were gradually replaced from margins by goethite (Fig. 10a) rarely with disseminated cinnabar.

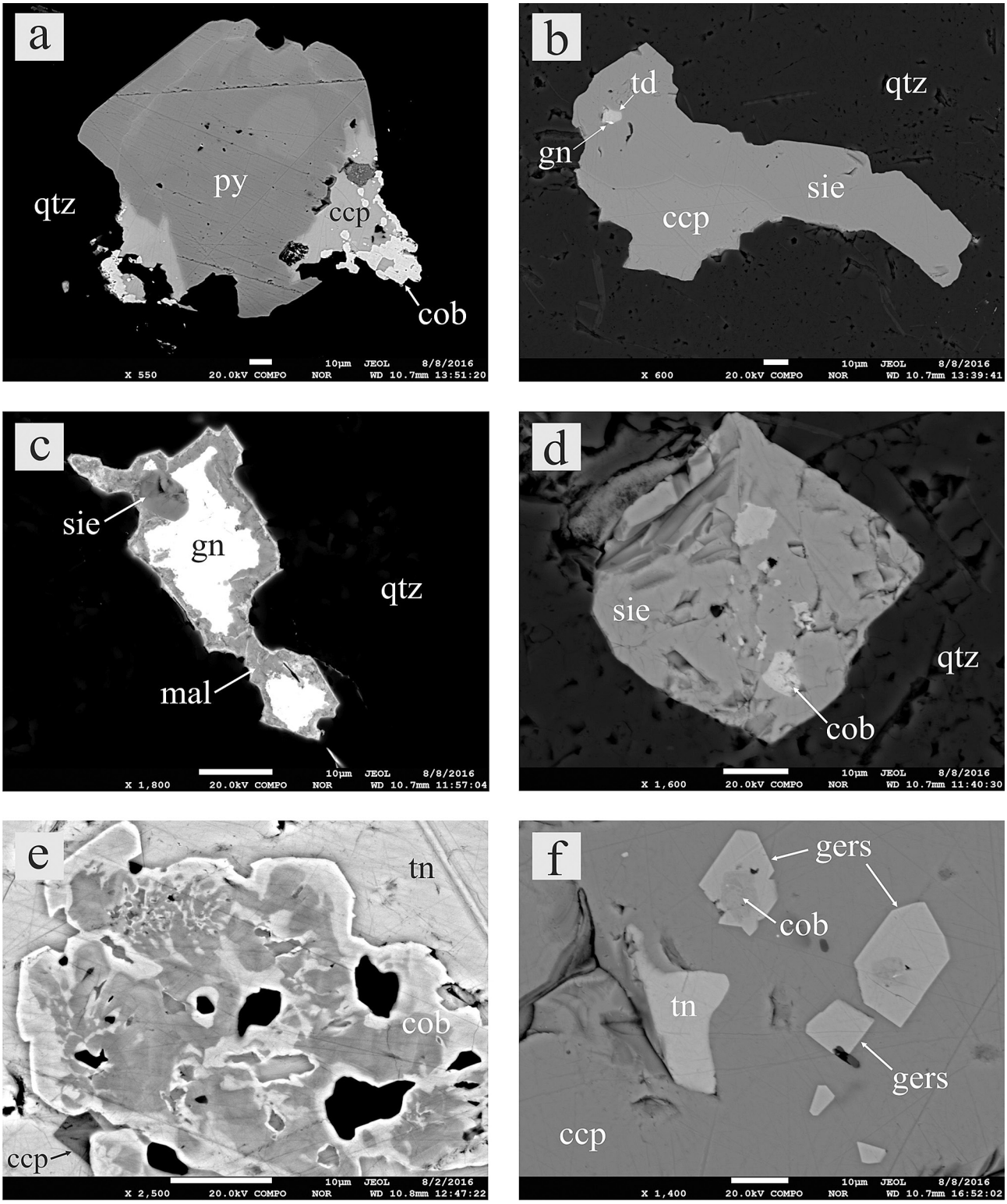

Fig. 5. a) Aggregate of zonal pyrite (py), chalcopyrite (ccp) and cobaltite (cob) in quartz (qtz); **b)** tetrahedrite and galena enclosed in siegenite and chalcopyrite; **c)** galena (gn) in association with siegenite (sie) is enclosed in quartz (qtz), galena peripheral parts are replaced by malachite (mal); **d)** aggregate of siegenite (sie) and cobaltite (cob) in quartz (qtz); **e)** diffusive inhomogeneous cobaltite in association with chalcopyrite (ccp) enclosed in tennantite; **f)** small grains of tennantite (tn), gersdorffite (gers) and cobaltite (cob) in chalcopyrite (ccp). (BSE)

Cobaltite-gersdorffite was observed as small inclusions (<50 μm) in tennantite where it occurs always in paragenetic association with chalcopyrite (Fig. 4e). These grains are often zonal in BSE imaging. Smaller crystals have simple zoning with dark center and bright border, or rarely with few darker stripes in lighter mass. Larger crystals exhibit unusual diffusive

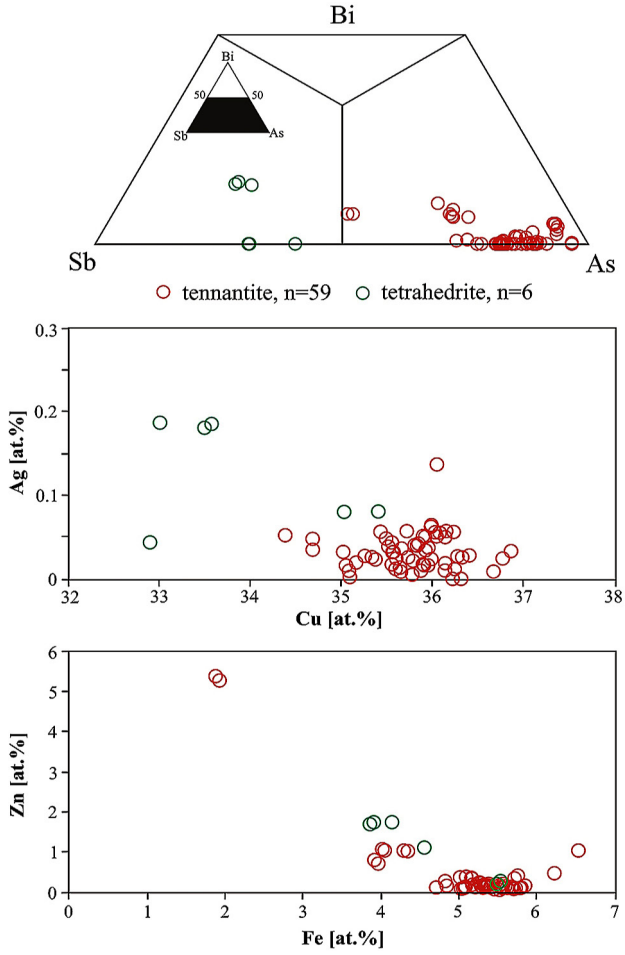

Fig. 6. Projection of analyses of tennantite and tetrahedrite in the Sb-As-Bi ternary system. Correlation between Ag-Cu and Zn-Fe content in tennantite and tetrahedrite (in at. %).

sector zoning (Fig. 5e). In most cases, zoning is caused by the variations of the As/S ratio. Cobaltite-gersdorffite was also found enclosed in chalcopyrite in the form of small euhedral or anhedral crystals (<20 μm) scattered (Fig. 4f) or arranged into chains in paragenetic association with pyrite (Fig. 4b). Zonal euhedral crystals have cobaltite cores and gersdorffite rims (Fig. 5f). Electron microprobe analyses confirmed wide variations of substitutions (Tab. 4, Fig. 7) of main elements in wt. %: Co: 7.1–32.7 (0.20–0.85 apfu); Ni: 1.5–24.1 (0.04-0.67 apfu); Fe: 1.0–8.8 (0.03–0.23 apfu); As: 27.2–50.5 (0.54–1.19 apfu); and S: 15.4–31.3 (0.85–1.44 apfu). Content of Cu varies in the range of 0.0–3.1 (7.3) wt. % (up to 0.19 apfu). Content of other elements (Pb, Sb, Bi, Ag, Se, Au) does not reach 0.3 wt. %. Chemical formula of Co- or Ni-richest members calculated on the basis of 3 atoms is $(Co_{0.85}Ni_{0.04}Fe_{0.10}Cu_{0.01})_{1.00}As_{0.73}S_{1.26}$ and $(Ni_{0.67}Co_{0.22}Fe_{0.07}Cu_{0.03})_{0.99}As_{1.03}S_{0.98}$, respectively. Substitution takes place between As and S, Co and Ni (Fig. 8). Strong negative correlation occurs between Fe+Cu and Co+Ni (Fig. 8). Much weaker positive or negative correlations were observed for As/S vs. Ni and As/S vs. Co, As/S vs. Fe, respectively.

Siegenite is rare mineral at the Podlipa. It occurs in association with tetrahedrite, galena, and chalcopyrite (Fig. 5b) or with quartz in the form of isometric or irregular grains. In one case, the relationship between cobaltite and siegenite was observed where siegenite replaces cobaltite (Fig. 5d). The content of Ni varies from 25.9 to 31.4 wt. % (1.36–1.67 apfu) and Co from 20.0 to 25.5 wt. % (1.21–1.34 apfu) (Tab. 4, Fig. 7). There is other group of analyses with higher content of Ni (~36 wt. %) but the analytical sums are lower due to the small size of the crystal (around 97 wt. %). Contents of other elements vary as follows in wt. %: Cu: 1.5–3.8 (up to 0.18 apfu), Bi: 0–1.5 (up to 0.02 apfu), Fe: 1.1–2.5 (up to 0.14 apfu) (Tab. 4). An average chemical formula, calculated on the base of 7 atoms is: $(Ni_{1.67}Co_{1.06}Fe_{0.14}Cu_{0.08}Bi_{0.02})_{2.97}S_{4.03}$.

Kupčíkite is a rare Bi-sulphosalt at the locality. It is associated with chalcopyrite and tennantite or tetrahedrite (Fig. 4d). Kupčíkite forms irregular grains up to 100 μm. It is chemically homogeneous, weak sector zoning was observed only in a single case and was caused by slight variations of Bi content. Our kupčíkite shows higher content of Fe (up to 0.56 apfu). Ag content is low (up to 0.05 apfu) what is typical for kupčíkite. Chemical formula was based on 19 atoms: $(Cu_{3.59}Fe_{0.52}$

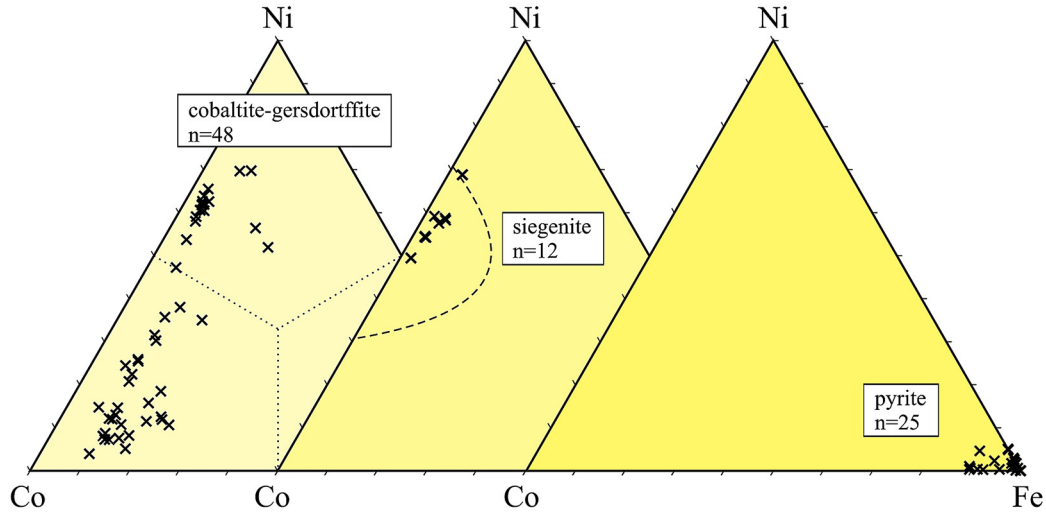

Fig. 7. Projection of analyses of sulphides and sulphoarsenides in the Co-Fe-Ni ternary system. Dashed line, in the middle triangle delimitates field of siegenite analyses summarized in Borichanskaya et al. (1981).

Tab. 2. Representative microprobe analyses of tennantite and tetrahedrite from the Podlipa deposit samples (bdl - below the detection limit). Analyse spots with 5, 6, 9 are identical to points of Raman spectroscopy acquisition.

Mineral	tennantite								tetrahedrite	
Analysis	1.	2.	3.	4.	5.	6.	7.	8.	9.	10.
Number	LP-1/15	L-100/15	P-6B/15A	HLP-6B/15	PO-65/14	LB-1/11	LB-301/15	LB- 304/15	LB-12/11	LB-19/11
	wt. %									
Cu	45.03	45.16	43.57	43.38	40.25	43.49	44.08	42.23	36.41	38.77
Sb	1.38	1.13	5.71	4.34	13.40	2.73	3.41	6.49	18.47	16.76
As	17.97	19.00	16.33	17.18	9.00	17.92	18.06	13.53	3.68	6.94
Zn	0.16	1.35	0.19	0.45	6.42	0.19	0.17	0.46	1.95	1.36
Fe	5.12	4.44	5.59	6.08	1.91	5.51	5.99	5.41	3.73	4.72
Ag	bdl	0.12	bdl	0.08	0.07	0.06	0.08	0.12	0.34	0.09
Pb	0.13	0.12	bdl	0.00	0.09	0.15	0.15	0.04	0.02	0.42
Hg	0.00	bdl	0.12	0.06	bdl	0.00	0.07	0.00	0.57	0.06
Bi	2.30	bdl	0.00	1.01	3.75	0.05	0.62	3.31	7.04	0.00
Cd	bdl	bdl	bdl	-	bdl	0.01	0.02	2.23	0.08	0.05
S	28.22	28.46	27.71	26.80	25.99	28.60	27.37	26.81	25.23	26.85
Se	0.00	0.20	0.22	0.00	0.00	-	0.00	0.00	0.00	0.00
Mn	0.00	0.00	-	-	0.00	-	-	-	-	0.00
Co	-	-	0.15	-	-	-	0.06	-	0.52	*2.21
Ni	-	-	0.05	-	-	-	0.00	-	0.00	*1.79
Sn	-	-	0.03	-	-	-	0.00	-	-	-
Total	**100.31**	**99.98**	**99.68**	**99.38**	**100.00**	**98.70**	**100.08**	**100.62**	**98.02**	**100.00**
	apfu, based on 29 atoms									
Cu	10.56	10.48	10.33	10.39	10.06	10.22	10.41	10.28	9.74	9.54
Sb	0.17	0.14	0.71	0.54	1.75	0.34	0.42	0.82	2.58	2.15
As	3.57	3.74	3.28	3.49	1.91	3.57	3.62	2.79	0.83	1.45
Zn	0.04	0.30	0.04	0.10	1.56	0.04	0.04	0.11	0.51	0.33
Fe	1.37	1.17	1.51	1.66	0.54	1.47	1.61	1.50	1.13	1.32
Ag	bdl	0.02	bdl	0.01	0.01	0.01	0.01	0.02	0.05	0.01
Pb	0.01	0.01	bdl	0.00	0.01	0.01	0.01	0.00	0.00	0.03
Hg	0.00	bdl	0.01	0.00	bdl	0.00	0.00	0.00	0.05	0.00
Bi	0.16	bdl	0.00	0.07	0.29	0.00	0.04	0.25	0.57	0.00
Cd	bdl	bdl	bdl	0.00	bdl	0.00	0.00	0.31	0.01	0.01
S	13.12	13.10	13.02	12.73	12.88	13.33	12.81	12.93	13.38	13.10
Se	0.00	0.04	0.04	0.00	0.00	-	0.00	0.00	0.00	0.00
Mn	0.00	0.00	-	-	0.00	-	-	-	-	0.00
Co	-	-	0.04	-	-	-	0.02	-	0.15	*0.59
Ni	-	-	0.01	-	-	-	0.00	-	0.00	*0.48
Sn	-	-	0.00	-	-	-	0.00	-	-	-
Sb/(Sb+As)	0.05	0.04	0.18	0.13	0.48	0.09	0.10	0.23	0.76	0.60

(*) – probably contaminated analysis

$Ag_{0.05}Cd_{0.01})_{4.17}(Bi_{4.94}Sb_{0.01})_{4.95}S_{9.89}$. Chemically calculated *N* for kupčíkite (Topa et al., 2003) is lower and varies from 0.81 to 0.94. Representative microprobe analyses are given in Tab. 5 and graphically shown in Fig. 9. Kupčíkite is rarely replaced by secondary minerals.

Matildite(?) was observed in one case under the electron microscope in the form of a tiny needle enclosed in quartz. Size of crystal (1 × 2 μm) allowed us to use the EDS analysis only. Chemical composition as follows is nearest to theoretical matildite: Ag: 30.49, Bi: 48.44, Cu: 3.28, S: 17.78 wt. %.

Galena is very rare. It occurs as small grain aggregates or short veinlets of size up to 30 μm in quartz or quartz-carbonate veins (Fig. 5c). It was identified by WDS analyses (Tab. 3) and contains up to 0.85 wt. % of Cu and 0.15 wt. % of Ag. Galena was also found as tiny inclusion in cobaltite and in paragenetic association with tetrahedrite enclosed in siegenite (Fig. 5b). Grains are replaced by secondary phases, probably malachite (EDS analysis: Cu, C) on the border parts.

Cinnabar is very rare mineral on the deposit, detected only by electron microscopy and EDS. It occurs in a form of tiny grains

on contact of pyrite with its Fe oxyhydroxide rims (Fig. 10a) and in massive botryoidal Fe oxyhydroxides (Fig. 10b). Chemical composition of cinnabar was determined by EDS analyses with Hg and S concentrations of 85.5 wt. % and 14.6 wt. %, respectively.

Gold was found in one sample. It occurs in the form of little grains of irregular elongated shape with a larger dimension of 15 μm (Fig. 11a) in association with quartz, enclosed in secondary minerals – goethite and pseudomalachite. Smaller grains fill little cracks (up to 1 μm thick) in secondary minerals (goethite). Chemical composition of the larger grain of gold is as follows (WDS analysis in wt. %): Au: 57.10, Ag: 30.82, Cu: 8.96, Fe: 1.43, Te: 0.30, Bi: 0.07, Hg: 0.10, Sum: 98.5.

Silver or Ag-S phases occur as small isolated grains up to 4 μm in diameter. Grains were found in cracks, vugs, but also in the mass of primary (tennantite, chalcopyrite, quartz) and secondary (pseudomalachite, goethite) minerals (Fig. 11b). EDS analysis confirmed presence of Ag, more often Ag and S. It was not possible to use more precise analysis due to small grains proportions. Position of silver suggests that it was remobilized from its primary source.

Cassiterite was observed in small amounts, but in many samples, as isolated grains or clusters. Grains mostly have isometric shape and reach up to 50 μm in diameter. Few observed crystals were cracked. Cassiterite grains are enclosed in chalcopyrite, quartz, K-mica or secondary minerals of Fe and Cu (Fig. 12a,b). Representative chemical composition detected by WDS analysis is: SnO_2: 98.94, CaO: 0.33, FeO: 0.50, MgO: 0.18, WO_3: 0.10, Sum: 100.05 wt. %.

Carbonates are accessory gangue minerals in the dump samples. They usually occur within hydrothermal quartz veins (Fig. 3) hosted in metaarkoses and are penetrated by younger quartz and sulphides (mainly chalcopyrite).

The minerals of **dolomite-ankerite** series are dominating among the carbonates. They are occurring as massive cracked and faulted crystals along their cleavage (Fig. 13), often strongly weathered or replaced by younger quartz (Fig. 13a). A characteristic feature is zoning corresponding to depletion in Fe, particularly in the aggregate rims and along the cracks (Fig. 13b). Growth oscillatory zoning is less abundant (Fig. 13c). Dolomite-ankerite aggregates are composed of $CaMg(CO_3)_2$ (from 62.39 to 87.49 mol. %), $CaFe(CO_3)_2$ (from 16.17 to 34.05 mol. %) and $CaMn(CO_3)_2$ (from 2.27 to 3.21 mol. %), compositions in dolomite-ankerite-kutnahorite system are presented in ternary diagram (Fig. 14). The aggregates are enriched in trace elements, content of SrO is up to 0.70 wt. %, concentration of BaO, SiO_2, Na_2O or Al_2O_3 is below 0.06 wt. % (Tab. 6). Carbonates of the dolomite group were confirmed by X-ray powder diffraction.

Siderite – only a few siderite grains were found in form of small columnar crystals of up to 50 μm in diameter, grown on the contact of dolomite with chalcopyrite fine veins penetrating into carbonates (Fig. 13d). Siderite is composed of $FeCO_3$ (from 76.60 to 78.82 mol. %), $MgCO_3$ (from 1.48 to 1.77 mol. %), $MnCO_3$ (from 17.00 to 18.33 mol. %), and $CaCO_3$ (from 2.70 to 3.30 mol. %) (Fig. 14, Tab. 7).

Calcite occurs very rarely. It was found as a part of massive dolomite-quartz vein, where it forms aggregate of euhedral

Tab. 3. Microprobe analyses of pyrite and galena (bdl - below the detection limit).

Mineral	pyrite										galena	
Analysis	1.	2.	3.	4.	5.	6.	7.	8.	9.	10.	1.	2.
Number	LP-1/15	LP-1/15	L-100/15	L-100/15	L-100/15	L-100/15	L-100/15	LB-301/15A	LB-301/15A	LB-19/11	LB-19/11	LB-19/11
	wt. %											
S	52.66	53.65	53.22	50.74	51.13	53.42	51.53	54.17	53.88	53.56	12.94	13.10
Fe	44.12	46.62	41.45	40.73	41.33	45.27	41.78	45.98	45.97	41.31	0.04	0.03
Pb	0.30	0.26	0.28	0.28	0.25	0.27	0.27	0.01	0.10	0.06	86.93	87.44
Ag	bdl	bdl	bdl	bdl	0.05	bdl	0.04	0.00	0.02	0.00	0.11	0.15
Sb	0.00	bdl	bdl	0.00	0.00	0.00	0.00	0.00	0.01	0.01	0.02	0.00
Bi	0.00	0.00	0.00	bdl	bdl	bdl	bdl	0.00	0.00	0.00	0.00	0.00
Cu	0.05	0.08	0.20	0.05	0.36	0.53	0.15	0.09	0.07	0.17	0.29	0.85
Ni	2.50	bdl	0.52	0.15	0.29	0.85	0.19	0.00	0.00	2.25	0.03	0.03
Co	bdl	bdl	4.85	4.93	4.85	0.50	4.16	0.07	0.06	2.92	0.00	0.01
Zn	0.00	0.00	0.00	0.00	0.00	0.00	0.00	0.00	0.00	0.03	0.03	0.00
Cd	-	-	-	-	-	-	-	0.02	0.05	0.03	0.01	0.02
As	bdl	bdl	0.00	3.47	2.44	bdl	1.83	0.00	0.00	0.29	0.06	0.07
Hg	0.00	0.00	0.00	0.00	0.00	0.00	0.00	0.00	0.00	0.02	0.03	0.00
Se	bdl	0.00	0.00	0.00	0.00	bdl	0.12	0.00	0.00	0.00	0.00	0.00
Au	bdl	bdl	0.00	0.00	0.00	0.00	0.00	-	-	-	-	-
Te	0.00	0.00	0.00	0.00	0.00	0.00	0.00	-	-	-	-	-
Sn	-	-	-	-	-	-	-	0.07	0.00	-	-	-
Total	99.63	100.61	100.54	100.35	100.70	100.83	100.07	100.40	100.16	100.64	100.48	101.69

Tab. 4. Microprobe analyses of sulphides and sulphoarsenides of Co-Ni-Fe (bdl - below the detection limit).

Mineral	siegenite						cobaltite-gersdorffite													
Analysis	1.	2.	3.	4.	5.	6.	1.	2.	3.	4.	5.	6.	7.	8.	9.	10.	11.	12.	13.	14.
Number	LB-19/11	LB-19/11	LB-19/11	LB-19/11	LB-19/11	LB-19/11	LP-1/15	P-6B/15	P-6B/15	HLP-6B/15	HLP-6B/15	LB-301/15	LB-301/15	LB-1/11	LB-1/11	LB-1/11	LB-X	LB-19/11	LB-19/11	LB-304/15
	wt. %						wt. %													
S	41.47	42.07	42.08	41.54	42.41	41.54	22.46	21.98	20.71	22.17	21.92	22.07	20.11	25.15	29.71	26.10	24.11	22.80	26.37	18.92
Ni	31.40	26.05	25.93	29.11	29.27	29.06	10.88	20.09	20.92	11.65	22.36	8.07	13.38	4.46	6.13	5.34	2.71	9.03	1.50	24.01
Co	19.98	25.53	25.47	23.12	23.15	23.15	21.47	10.51	11.35	21.92	13.09	25.06	17.96	28.67	26.60	27.40	30.35	25.38	32.69	7.07
Ag	0.00	0.00	0.00	0.00	0.00	0.00	bdl	0.00	0.01	0.00	0.00	0.00	0.00	-	-	-	-	0.00	0.00	0.00
Fe	2.47	1.08	1.11	1.45	1.28	1.30	3.53	1.48	1.11	3.29	1.42	3.10	3.63	3.45	5.94	3.60	4.43	2.47	3.60	3.20
Sb	0.00	0.00	0.00	0.00	0.00	0.00	0.00	0.88	0.06	0.00	0.00	0.00	0.00	bdl	bdl	0.10	bdl	0.00	0.00	0.03
Hg	0.00	0.00	0.00	0.00	0.03	0.00	0.00	0.00	0.00	0.00	0.00	0.00	0.00	-	-	-	-	0.00	0.00	0.00
As	0.00	0.01	0.00	0.00	0.00	0.00	41.26	37.06	45.72	41.00	41.57	42.34	45.44	36.42	30.11	35.29	37.64	41.25	35.65	46.18
Se	0.01	0.00	0.00	0.00	0.00	0.00	bdl	0.13	0.00	0.00	0.00	0.00	0.00	-	-	-	-	0.00	0.00	0.00
Bi	1.53	0.46	0.00	0.55	0.41	0.49	0.00	bdl	0.08	0.00	bdl	0.11	0.14	bdl	bdl	bdl	0.28	0.00	0.00	0.00
Cu	1.66	3.74	3.80	2.52	2.49	2.46	0.90	7.34	1.23	0.26	0.18	0.38	0.14	1.33	1.04	2.48	1.55	0.11	0.47	1.82
Zn	0.00	0.00	0.04	0.00	0.00	0.03	0.00	0.00	0.00	-	-	0.00	0.05	-	-	-	0.03	0.01	0.01	0.00
Cd	0.03	0.03	0.07	0.00	0.02	0.07	-	-	0.02	-	-	0.00	0.04	bdl	bdl	bdl	-	0.04	0.05	0.06
Pb	0.00	0.00	0.03	0.07	0.05	0.05	0.10	0.10	0.08	0.08	0.07	0.10	0.04	0.11	0.17	0.18	-	0.11	0.01	0.02
Au	-	-	-	-	-	-	0.00	0.00	-	0.00	0.00	-	-	-	-	-	0.00	-	-	-
Te	-	-	-	-	-	-	0.00	0.00	-	-	-	-	-	-	-	-	-	-	-	-
Sn	-	-	-	-	-	-	-	-	0.00	-	-	0.02	0.03	-	-	-	-	-	-	-
Total	98.57	98.97	98.52	98.36	99.12	98.14	100.59	99.57	101.28	100.37	100.62	101.25	100.96	99.58	99.70	100.50	101.10	101.20	100.35	101.29
	apfu, based on 7 atoms						apfu, based on 3 atoms													
S	4.03	4.05	4.05	4.03	4.06	4.03	1.12	1.11	1.05	1.11	1.10	1.10	1.02	1.23	1.38	1.25	1.17	1.13	1.26	0.97
Ni	1.67	1.37	1.36	1.54	1.53	1.54	0.30	0.55	0.58	0.32	0.61	0.22	0.37	0.12	0.16	0.14	0.07	0.24	0.04	0.67
Co	1.06	1.34	1.33	1.22	1.21	1.22	0.58	0.29	0.31	0.60	0.36	0.68	0.50	0.76	0.67	0.72	0.80	0.68	0.85	0.20
Ag	0.00	0.00	0.00	0.00	0.00	0.00	bdl	0.00	0.00	0.00	0.00	0.00	0.00	-	-	-	-	0.00	0.00	0.00
Fe	0.14	0.06	0.06	0.08	0.07	0.07	0.10	0.04	0.03	0.09	0.04	0.09	0.11	0.10	0.16	0.10	0.12	0.07	0.10	0.09
Sb	0.00	0.00	0.00	0.00	0.00	0.00	0.00	0.01	0.00	0.00	0.00	0.00	0.00	bdl	bdl	0.00	bdl	0.00	0.00	0.00
Hg	0.00	0.00	0.00	0.00	0.00	0.00	0.00	0.00	0.00	0.00	0.00	0.00	0.00	-	-	-	-	0.00	0.00	0.00
As	0.00	0.00	0.00	0.00	0.00	0.00	0.88	0.80	0.99	0.88	0.89	0.90	0.99	0.76	0.60	0.73	0.78	0.87	0.73	1.01
Se	0.00	0.00	0.00	0.00	0.00	0.00	bdl	0.00	0.00	0.00	0.00	0.00	0.00	-	-	-	-	0.00	0.00	0.00
Bi	0.02	0.01	0.00	0.01	0.01	0.01	0.00	bdl	0.00	0.00	0.00	0.00	0.00	bdl	bdl	bdl	0.00	0.00	0.00	0.00
Cu	0.08	0.18	0.18	0.12	0.12	0.12	0.02	0.19	0.03	0.01	0.00	0.01	0.00	0.03	0.02	0.06	0.04	0.00	0.01	0.05
Zn	0.00	0.00	0.00	0.00	0.00	0.00	0.00	0.00	0.00	-	-	0.00	0.00	-	-	-	0.00	0.00	0.00	0.00
Cd	0.00	0.00	0.00	0.00	0.00	0.00	-	-	0.00	-	-	0.00	0.00	bdl	bdl	bdl	-	0.00	0.00	0.00
Pb	0.00	0.00	0.00	0.00	0.00	0.00	0.00	0.00	0.00	0.00	0.00	0.00	0.00	0.00	0.00	0.18	-	0.00	0.00	0.00
Au	-	-	-	-	-	-	0.00	0.00	-	0.00	0.00	-	-	-	-	-	0.00	-	-	-
Te	-	-	-	-	-	-	0.00	0.00	-	-	-	-	-	-	-	-	-	-	-	-
Sn	-	-	-	-	-	-	-	-	0.00	-	-	0.00	0.00	-	-	-	-	-	-	-

crystals (in size up to 50 μm). It was identified by Raman spectroscopy (Tab. 8) and X-ray powder diffraction.

Dissolution of the carbonate minerals often left hollow spaces in quartz, later filled by pseudomalachite or other supergene minerals.

Quartz is the most common gangue mineral at the deposit. It has milky white to greyish white colour. There are several generations of quartz. It sometimes forms banded texture (Fig. 3). Sulphides intersecting older quartz bands are associated with younger quartz, forming small euhedral crystals in vugs.

4.3. Raman spectroscopy

4.3.1. Carbonates

Measured values of Raman shifts of selected carbonates were compared and assigned according to published data (Burke, 2001; Gunasekaran et al., 2006; Buzgar & Apopei, 2009; Frezzotti et al., 2012). Measurements on carbonates of known chemical composition have shown that dolomite Raman shifts are influenced by the relative proportions of the cations Ca^{2+}, Fe^{2+}, Mg^{2+}, and Mn^{2+}. Bands of the translation modes tend to shift to lower values in dolomites with high FeO content, while symmetric stretching of CO_3 group is shifted to higher frequencies (Tab. 8). Raman shifts for siderite and calcite from studied samples and their assignments are presented in Tab. 8. They are in a good agreement with published data for those minerals.

4.3.2. Tennatite-tetrahedrite

We inspected the potential of Raman spectroscopy for identification of the members of the tetrahedrite-tennantite solid solution (i.e. in the case of small grains, or rock samples). Two end-members of our sample set and one of intermediate composition were analysed. Raman spectra are shown in Fig. 15. The degree of As-Sb substitution is quantified by Sb/(Sb+As) ratios (Tab. 1). Bands in the range of 250–400 cm^{-1} correspond to 4 vibrational modes of trigonal pyramids XY_3, where X = As, Sb, Bi, and Y = S. The most intense band in the spectrum corresponds to ν_1 (A1) symmetric stretching (Nakamoto, 1997). High content of Sb (heavier element slows the bond vibration down) shifts this band to lower wavenumbers (363 cm^{-1}), high content of As (lighter element causes faster vibration) to higher ones (385 cm^{-1}). In the spectrum of the sample with intermediate composition, both bands appear. Similar feature can be

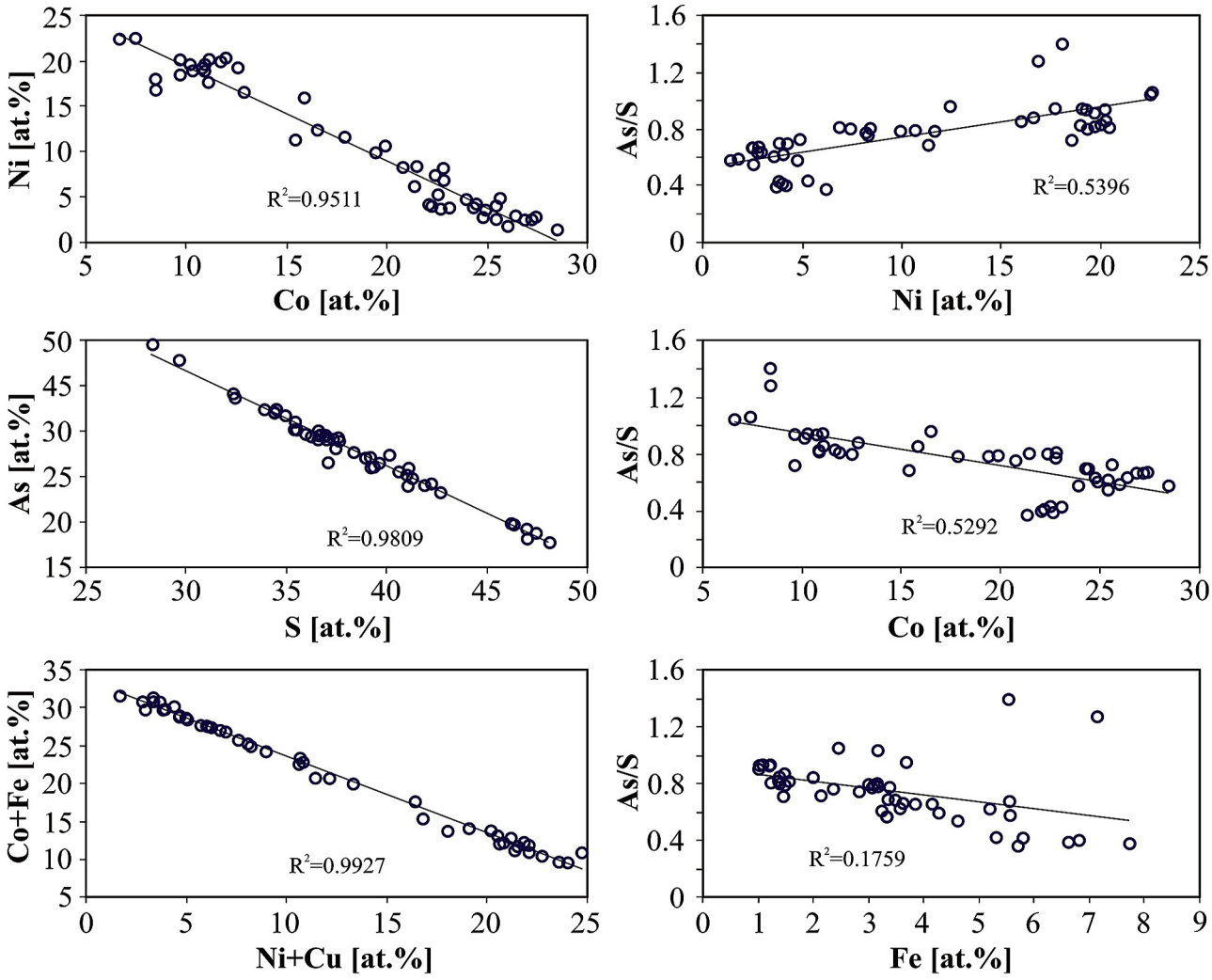

Fig. 8. Relationship between main chemical constituents of cobaltite-gersdorffite series.

Tab. 5. Microprobe analyses of kupčíkite.

Mineral	kupčíkite								
Analysis	1.	2.	3.	4.	5.	6.	7.	8.	9.
Number	LB-304/15	LB-304/15	LB-304/15	LB-304/15	LB-304/15	LB-304/15	LB-304/15	LB-304/15	LB-304/15
	wt. %								
Ag	0.34	0.33	0.27	0.20	0.08	0.16	0.03	0.02	0.10
Fe	1.85	1.81	1.81	1.83	1.95	1.76	1.90	1.75	1.92
Sb	0.05	0.04	0.06	0.03	0.02	0.03	0.06	0.06	0.05
Hg	0.00	0.00	0.00	0.00	0.00	0.00	0.00	0.00	0.00
As	0.00	0.00	0.00	0.00	0.00	0.00	0.00	0.00	0.00
Se	0.00	0.00	0.00	0.00	0.00	0.00	0.00	0.00	0.00
Bi	63.40	64.73	63.09	62.72	63.76	63.00	65.71	62.66	63.85
Cu	14.42	14.28	14.39	14.41	14.38	14.71	14.31	14.31	14.34
Ni	0.00	0.01	0.01	0.02	0.00	0.00	0.00	0.01	0.02
Co	0.00	0.00	0.00	0.00	0.00	0.00	0.00	0.01	0.02
S	19.40	19.86	19.51	19.36	19.63	19.46	19.52	19.57	20.00
Zn	0.00	0.00	0.03	0.00	0.02	0.04	0.00	0.00	0.01
Cd	0.09	0.07	0.06	0.03	0.03	0.05	0.08	0.08	0.00
Pb	0.00	0.00	0.00	0.00	0.00	0.00	0.00	0.00	0.00
Total	99.54	101.12	99.22	98.60	99.87	99.21	101.60	98.45	100.30
	apfu, based on 19 atoms								
Ag	0.05	0.05	0.04	0.03	0.01	0.02	0.00	0.00	0.02
Fe	0.54	0.52	0.52	0.53	0.56	0.51	0.54	0.51	0.55
Sb	0.01	0.01	0.01	0.00	0.00	0.00	0.01	0.01	0.01
Hg	0.00	0.00	0.00	0.00	0.00	0.00	0.00	0.00	0.00
As	0.00	0.00	0.00	0.00	0.00	0.00	0.00	0.00	0.00
Se	0.00	0.00	0.00	0.00	0.00	0.00	0.00	0.00	0.00
Bi	4.92	4.94	4.89	4.89	4.91	4.88	5.05	4.88	4.87
Cu	3.68	3.59	3.67	3.69	3.64	3.75	3.61	3.66	3.60
Ni	0.00	0.00	0.00	0.01	0.00	0.00	0.00	0.00	0.00
Co	0.00	0.00	0.00	0.00	0.00	0.00	0.00	0.00	0.00
S	9.80	9.89	9.85	9.84	9.86	9.82	9.77	9.92	9.95
Zn	0.00	0.00	0.01	0.00	0.00	0.01	0.00	0.00	0.00
Cd	0.01	0.01	0.01	0.00	0.00	0.01	0.01	0.01	0.00
Pb	0.00	0.00	0.00	0.00	0.00	0.00	0.00	0.00	0.00
N	0.87	0.94	0.86	0.83	0.85	0.81	0.94	0.85	0.86

observed in lattice vibrations (< 200 cm^{-1}), where tetrahedrite has a band around 114 cm^{-1} while tennantite around 137 cm^{-1}. More detailed information on assignment of vibrational modes to band positions in tetrahedrite-tennantite can be found in Kharbish et al. (2007).

4.3.3. Stable isotopes

We analysed 15 samples of chalcopyrite and 2 samples of tennantite for sulphur isotope composition. Values of $\delta^{34}S$ in chalcopyrite vary in the range of 6.69–9.77 ‰ CDT (Tab. 9). Equilibrium isotope fractionation between chalcopyrite and H_2S in coexisting fluid in temperature range 100–300 °C is between 0.36 and 0.15 permil (fractionation factors of Li & Liu, 2006), which is almost within the range of analytical uncertainty. Thus, the measured isotope values are roughly representing fluid composition, overestimated by mentioned fractionation. Values of $\delta^{34}S$ in tennantite fall within the range of those measured in chalcopyrite. Unfortunately, the fractionation factors for tennantite-H_2S were not published yet.

5. DISCUSSION

Minerals of tetrahedrite-tennantite series occasionally with higher content of Bi and Au were reported from the Podlipa deposit (Koděra (Ed.), 1990; Slavkay et al., 2004, and references therein). In our samples, tennantite predominates over tetrahedrite distinctly. Fe prevails in divalent metals and excess of Cu suggests its presence in the divalent form in tetrahedral coordination. Content of Ag is very low. As prevails over Sb in trivalent cations. Higher content of Bi was detected in some samples. Similar characteristics of tennantite were determined at the nearby localities Svätodušná and Kolba (Michňová, 2009). Tennantite and tetrahedrite were reported also from Špania Dolina by Michňová (2009) and Sejkora et al. (2013). In the cobaltite-gersdorffite series, the Co-Ni substitution (Fig. 7) spans almost the entire solid solution. However, dry mineral synthesis in Co-Ni-Fe-As-S system (Klemm, 1965; Hem & Makovicky, 2004) suggest that such Co-Ni substitution in these minerals is possible only at higher

temperatures (> 500–600 °C) which are very unlikely for the Podlipa deposit. Possibly in natural conditions where the time factor is not as restrictive as in laboratory experiments the solid solution may be stable even at lower temperatures. Observed minerals are zoned (in BSE), but they occur in the same position separately (gersdorffite+chalcopyrite in tennantite, cobaltite+chalcopyrite in tennantite). Zoning is caused by variations of As and S content, where cores are enriched in S and rims in As. Usually increase in As is accompanied with Ni-enrichment. Only in a single instance, there is a grain with cobaltite core and gersdorffite rim (Fig. 5f).

Minerals of cobaltite-gersdorffite series from the Podlipa deposit are not mentioned in literature, though they were reported from the near Svätodušná and Kolba occurrences (Láznička, 1966; Koděra (Ed.), 1990; Michňová, 2009). Arsenopyrite, described by Hauerová et al. (1989), was not detected in our samples. All analysed grains with rhombic shape by electron microprobe and Raman spectroscopy fit to pyrite.

Primary mineral of Bi has not been reported from the Podlipa yet, only tetrahedrite with higher content of Bi (Slavkay et al., 2004). Bi sulphosalts (bismuthinite, pekoite, gladite, unknown phases, kobelite) in association with tennantite,

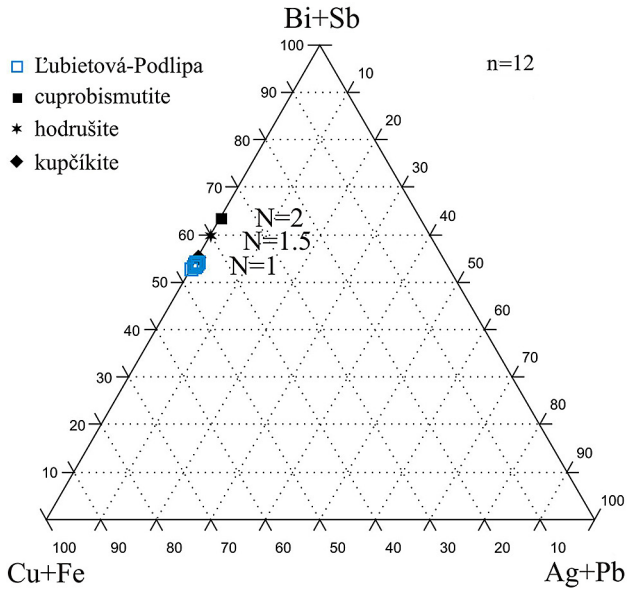

Fig. 9. Ternary diagram of Bi sulphosalts of cuprobismutite homologous series with analyses of kupčíkite from Ľubietová-Podlipa deposit. N means chemical number of the homologue.

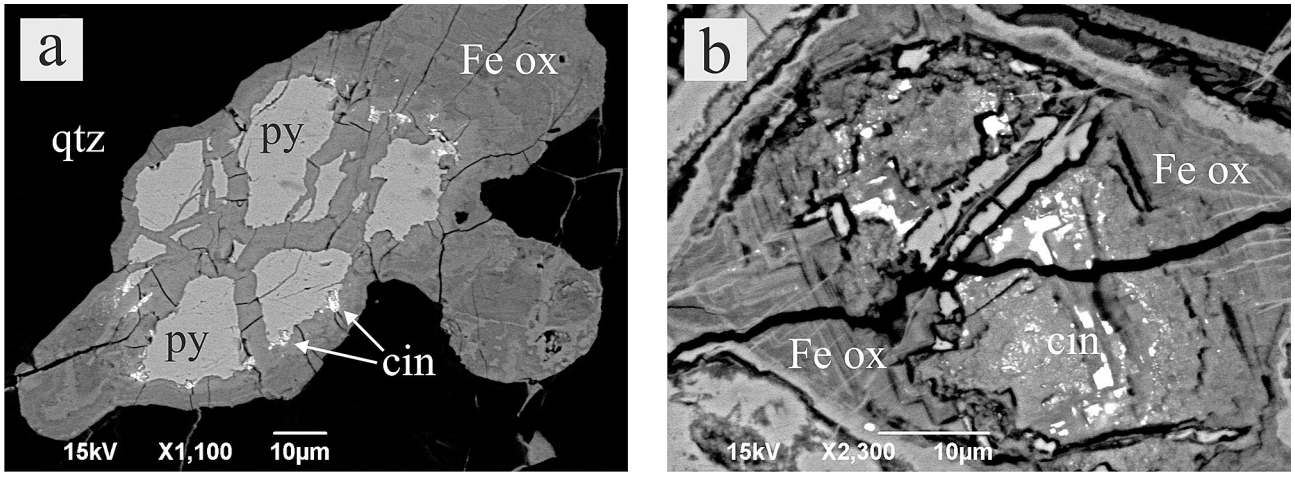

Fig. 10. a) Cinnabar (cin) grains on contact of pyrite (py) and zonal Fe oxyhydroxides (Fe ox); **b)** finely grained aggregate of cinnabar (cin) in zonal massive Fe oxyhydroxides (Fe ox). (BSE)

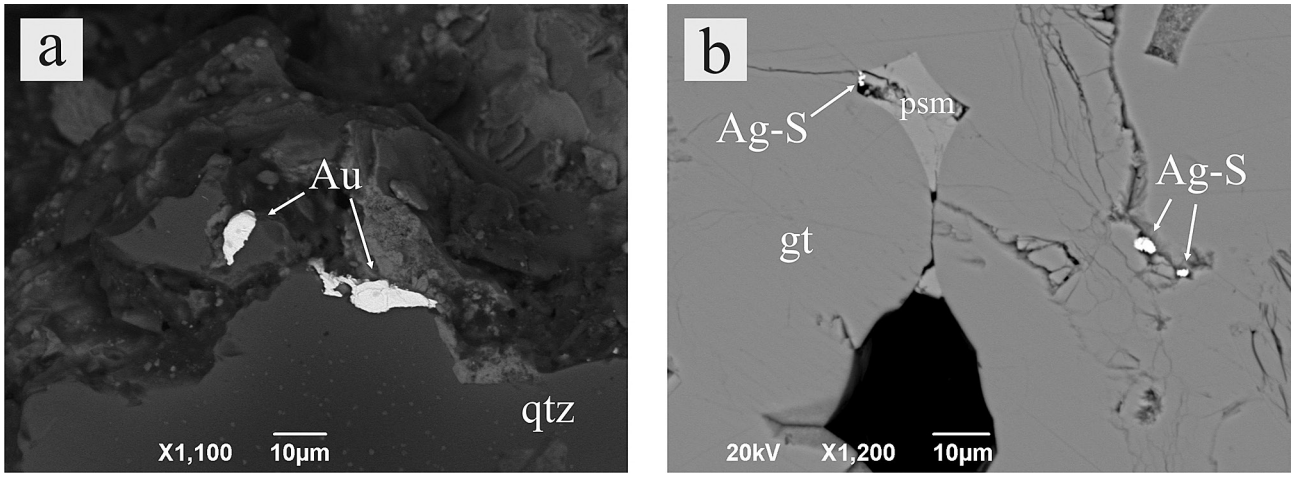

Fig 11. a) Grains of gold (Au) in association with quartz (qtz); **b)** grains of Ag-S traped in secondary minerals, goethite (gt) and pseudomalachite (psm). (BSE)

Tab. 6. Microprobe analyses and crystalochemical formula of the minerals of the dolomite-ankerite series from the Podlipa deposit.

	Dolomite-ankerite – chemical composition (wt. %) and crystalochemical formula, samples LB-304/15 (an. 1–12) and LB-300/15 (an. 13–15)										
Analysis Number	CaO	MgO	FeO	MnO	BaO	SiO_2	Na_2O	Al_2O_3	SrO	CO_2	Total
1	28.25	13.10	11.30	1.12	0.00	0.00	0.00	0.02	0.60	44.38	**98.77**
2	28.17	14.38	9.64	0.95	0.00	0.00	0.05	0.00	0.35	44.49	**98.04**
3	28.16	13.59	10.39	1.30	0.00	0.00	0.02	0.02	0.66	44.17	**98.31**
4	28.17	14.54	9.04	1.04	0.02	0.06	0.01	0.00	0.47	44.79	**98.14**
5	28.26	14.65	9.15	1.15	0.02	0.01	0.00	0.02	0.46	44.51	**98.23**
6	28.18	13.76	10.35	1.07	0.00	0.01	0.00	0.00	0.39	44.42	**98.19**
7	28.33	14.33	9.45	1.10	0.00	0.04	0.00	0.00	0.38	44.51	**98.14**
8	28.05	14.75	9.04	1.00	0.03	0.00	0.00	0.00	0.70	44.63	**98.20**
9	28.00	12.83	11.45	1.16	0.00	0.02	0.00	0.02	0.59	44.01	**98.07**
10	28.31	15.64	7.80	0.99	0.02	0.00	0.00	0.01	0.57	44.74	**98.07**
11	27.94	13.22	11.14	1.18	0.00	0.00	0.00	0.00	0.54	44.14	**98.16**
12	27.97	13.10	11.49	1.14	0.00	0.00	0.03	0.02	0.62	44.30	**98.66**
13	28.47	16.21	7.22	0.99	0.00	0.03	0.00	0.00	0.20	44.90	**98.03**
14	28.49	15.68	7.40	1.16	0.00	0.05	0.05	0.00	0.42	44.79	**98.04**
15	28.71	15.58	7.42	1.12	0.00	0.06	0.01	0.00	0.40	44.84	**98.13**
1	$Ca_{1.00}(Mg_{0.65}Fe_{0.31}Mn_{0.03}Sr_{0.01})_{1.00}(CO_3)_2$										
2	$Ca_{0.99}(Mg_{0.71}Fe_{0.27}Mn_{0.03}Sr_{0.01})_{1.01}(CO_3)_2$										
3	$Ca_{1.00}(Mg_{0.67}Fe_{0.29}Mn_{0.04}Sr_{0.01})_{1.00}(CO_3)_2$										
4	$Ca_{1.00}(Mg_{0.72}Fe_{0.25}Mn_{0.03}Sr_{0.01})_{1.00}(CO_3)_2$										
5	$Ca_{0.99}(Mg_{0.72}Fe_{0.25}Mn_{0.03}Sr_{0.01})_{1.01}(CO_3)_2$										
6	$Ca_{1.00}(Mg_{0.68}Fe_{0.29}Mn_{0.03}Sr_{0.01})_{1.00}(CO_3)_2$										
7	$Ca_{1.00}(Mg_{0.70}Fe_{0.26}Mn_{0.03}Sr_{0.01})_{1.00}(CO_3)_2$										
8	$Ca_{0.99}(Mg_{0.72}Fe_{0.25}Mn_{0.03}Sr_{0.01})_{1.01}(CO_3)_2$										
9	$Ca_{1.00}(Mg_{0.64}Fe_{0.32}Mn_{0.03}Sr_{0.01})_{1.00}(CO_3)_2$										
10	$Ca_{0.99}(Mg_{0.76}Fe_{0.21}Mn_{0.03}Sr_{0.01})_{1.01}(CO_3)_2$										
11	$Ca_{0.99}(Mg_{0.65}Fe_{0.31}Mn_{0.03}Sr_{0.01})_{1.01}(CO_3)_2$										
12	$Ca_{0.99}(Mg_{0.65}Fe_{0.32}Mn_{0.03}Sr_{0.01})_{1.01}(CO_3)_2$										
13	$Ca_{0.99}(Mg_{0.78}Fe_{0.20}Mn_{0.03}Sr_{0.00})_{1.01}(CO_3)_2$										
14	$Ca_{1.00}(Mg_{0.76}Fe_{0.20}Mn_{0.03}Sr_{0.01})_{1.00}(CO_3)_2$										
15	$Ca_{1.00}(Mg_{0.76}Fe_{0.20}Mn_{0.03}Sr_{0.01})_{1.00}(CO_3)_2$										

Tab. 7. Microprobe analyses and crystalochemical formula of siderite from the Podlipa deposit.

	Siderite - chemical composition (wt. %) and crystalochemical formula, sample L-100/15										
Analysis number	CaO	MgO	FeO	MnO	BaO	SiO_2	Na_2O	Al_2O_3	SrO	CO_2	Total
1	1.47	0.48	47.70	11.23	-	-	-	-	-	37.86	**98.74**
2	1.21	0.40	49.10	10.42	-	-	-	-	-	37.92	**99.04**
3	1.46	0.45	46.94	11.53	0.00	0.03	0.00	0.01	0.00	37.60	**98.02**
4	1.33	0.45	47.87	11.04	0.00	0.00	0.02	0.00	0.01	37.72	**98.43**
5	1.16	0.39	48.81	10.67	0.00	0.02	0.00	0.00	0.03	37.90	**98.97**
1	$(Fe_{0.77}Mn_{0.18}Mg_{0.01}Ca_{0.03})CO_3$										
2	$(Fe_{0.79}Mn_{0.17}Mg_{0.01}Ca_{0.02})CO_3$										
3	$(Fe_{0.77}Mn_{0.19}Mg_{0.01}Ca_{0.03})CO_3$										
4	$(Fe_{0.78}Mn_{0.18}Mg_{0.01}Ca_{0.03})CO_3$										
5	$(Fe_{0.79}Mn_{0.17}Mg_{0.01}Ca_{0.02})CO_3$										

chalcopyrite, quartz, carbonates and older Fe-Ni-Co sulphoarsenides were found at the near locality Ľubietová-Kolba (Pršek & Mikuš, 2006). Secondary bismuth minerals identified at the Podlipa such as mrázekite (Řídkošil et al., 1992) and bismutite (Milovská et al., 2014) imply that sulphides other than tennantite-tetrahedrite may contain Bi as a major element. Kupčíkite was identified as a rare mineral at the Podlipa. Chemical *N* (order of the homologue of cuprobismutite homologous series) of theoretical kupčíkite is equal to 1, our values are lower (0.81–0.94), possibly as a result of Cu-Bi substitution (Topa et al., 2003.). Kupčíkite was reported only from two other localities in the Western Carpathians – Čierna Lehota (Mikuš et al., 2002; Pršek et al., 2005) and Rozália Mine, Hodruša-Hámre (Jeleň et al., 2012; Sejkora et al., 2015). At Čierna Lehota, it has increased Fe content and occurs with other members of cuprobismutite homologous series in association with tennantite, chalcopyrite, sphalerite, matildite, and Ni-As-Bi minerals in black shales. At the Rozália Mine, kupčíkite belongs to hydrothermal base-metal mineralization and occurs as tiny sporadic grains in association with matildite, emplectite, and wittichenite in chalcopyrite–hematite aggregates, or as intergrowths with hodrušite, paděraite and members of the bismuthinite–aikinite series. Most commonly, it forms lamellae with emplectite, hodrušite, and krupkaite (Jeleň et al., 2012).

The carbonates siderite, ankerite, and dolomite were already described at the Podlipa deposit (Hvožďara, 1971; Ilavský et al., 1978; Hauerová et al., 1989; Koděra (Ed.), 1990; Slavkay et al., 2004). Data from this study show for occurrence of Fe-bearing dolomite with ankerite zones, siderite, and calcite. Dolomite-ankerite from the Podlipa samples is chemically similar to the carbonates from the Svätodušná and Kolba deposits (cf. Michňová, 2009), except of higher

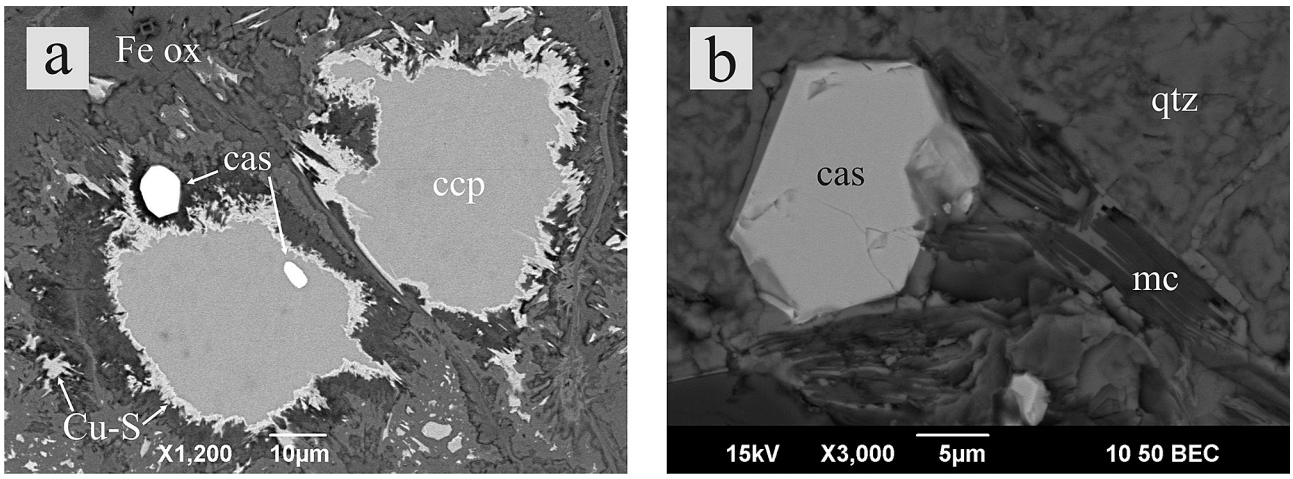

Fig. 12. a) Euhedral grains of cassiterite (cas) enclosed in chlacopyrite (ccp) and Fe oxyhydroxides (Fe ox); **b)** cassiterite (cas) in association with quartz (qtz) and mica (mc). (BSE)

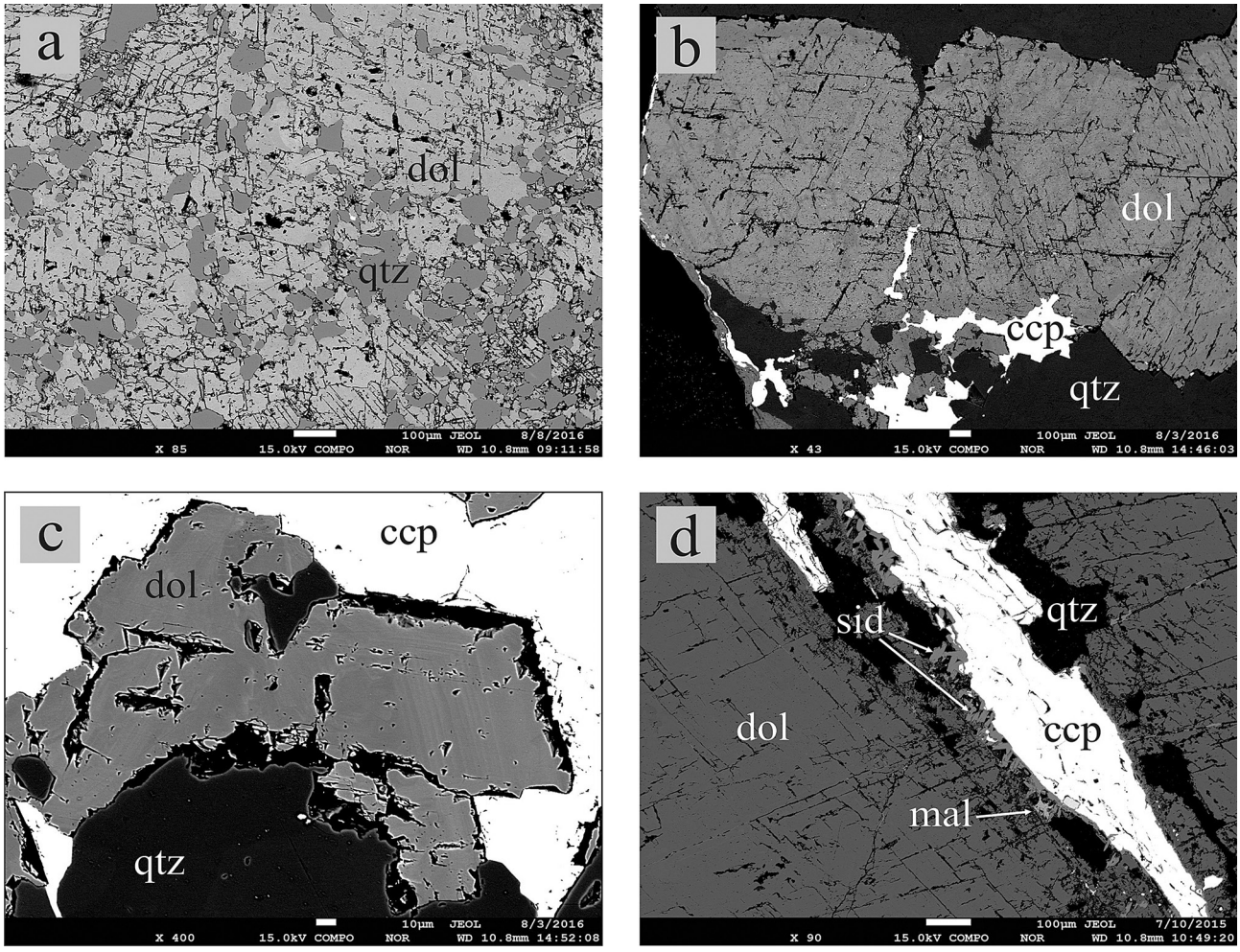

Fig. 13. a) Mineral association: old massive dolomite (dol) and probably newly equeled quartz (qtz) grains; **b)** cracked zonal dolomite (dol) aggregate and chalcopyrite (ccp) veinlets in quartz (qtz); **c)** dolomite (dol) crystals with visible growth zonation, in association with quartz (qtz) and chalcopyrite (ccp); **d)** veinlet of chalcopyrite (ccp) penetrating into cracked dolomite (dol), with small siderite (sid) crystals on their contact. (BSE)

MnO contents in the Kolba samples. Although Raman spectra of carbonate minerals are not uncommon in literature, they are very rarely paired with chemical composition, which is important in the solid solutions in system $CaMn(CO_3)_2$ – $CaMg(CO_3)_2$ – $CaFe(CO_3)_2$ especially for near end-members. It is thus hardly possible to correlate shifts in Raman bands

Tab. 8. Values of Raman shifts for minerals of dolomite-ankerite series, siderite and calcite.

		Assignment and Raman shift (cm^{-1})					
Carbonate minerals	**Sample**	**T(Fe, CO_3)**	**T(Fe, CO_3)**	**v_4**	**v_1**	**v_3**	**$v_1 + v_4$**
Dolomite (10.39 wt. % FeO)	thin section	173	293	724	1096	1442	1755
Dolomite (9.04 wt. % FeO)	thin section	173	294	723	1096	1438-1443	1754
Dolomite (7.40 wt. % FeO)	thin section	174	296	723	1097	1442	1758
Siderite (47.69-49.10 wt.% FeO)	thin section	184	285	733	1087	-	1726
Calcite (not estimated)	rock sample	154	281	712	1086	1435	1748

T - translations modes between the cation and CO_3 group, v_1 – symmetric CO_3 stretching, v_3 – asymmetric CO_3 stretching, v_4 – in-plane symmetric bending of CO_3

Tab. 9. Sulphur isotope composition in chalcopyrite and tennantite.

Sample	Mineral/occurence	$\delta^{34}S_{CDT}$
LB-2/11	ccp	9.77
LP-1/15A	ccp	8.79
LP-1/15B	ccp	8.72
LB-301/15A	ccp	8.88
LB-301/15B	ccp	7.80
LB-302/15	ccp	7.87
LS-1/16	ccp	6.97
LS-5/16z	ccp /vein	7.13
LS-5/16r	ccp /disseminated	6.69
LS-6/16	ccp	6.74
LS-8/16	ccp	7.30
LS-9/16	ccp	7.69
LS-12/16B	ccp	7.70
LS-12/16A	ccp	7.61
LS-7/16	ccp	7.68
LS-7/16	tn	7.55
P-6B	tn	8.81

ccp – chalcopyrite, tn – tennantite

to cation composition. In our samples, the Fe content seems to covariate with lattice vibrations – decrease in vibrational frequency is observed with increasing Fe concentration, i.e. mass of the cation. Siderite enriched in Mn could be a potential source of manganese in the ubiquitous secondary Mn-oxides, since no other primary Mn-bearing mineral was found in the deposit except for the scarce siderite.

Native metals, Au and Ag (and Ag-S) and HgS are probably products of remobilization and secondary precipitation in the cementation zone.

Cassiterite was not described from the Podlipa in earlier works (cited above) and its origin remains unclear. It was observed *(a)* in association with euhedral quartz and coarse-grained K-mica, or *(b)* embedded in chalcopyrite and secondary minerals. This may be indicative of its early crystallization during pre-sulphidic phase of deposit evolution (Stage 3 of Ozdín et al., 2016). We can tentatively relate it to Permian acidic effusives occurring in close vicinity of the deposit, or to host metasediments rich in granitic clastic material (Vozárová & Vozár, 1988). These rocks may have served as a source of Sn for fluids. On the other hand, it should be noted that granitic rocks of Veporic Superunit do not show particularly high concentrations of Sn (up to 11 ppm, Slavkay et al., 2004).

Previous authors mention presence of primary hematite (Hauerová et al., 1989). We observed hematite as platy grains crystallized on secondary Mn-oxides or enclosed in Cu carbonates. Hematite in this position is considered to be secondary in origin.

Sulphur stable isotope composition of Cu-sulphides varies in a tight range of 3.08 ‰ around a median value 7.69 ‰. Such a small range suggests a sulphur source from a homogenous reservoir than mixing of multiple sources. The relatively heavy isotopic composition and narrow range also excludes biogenic

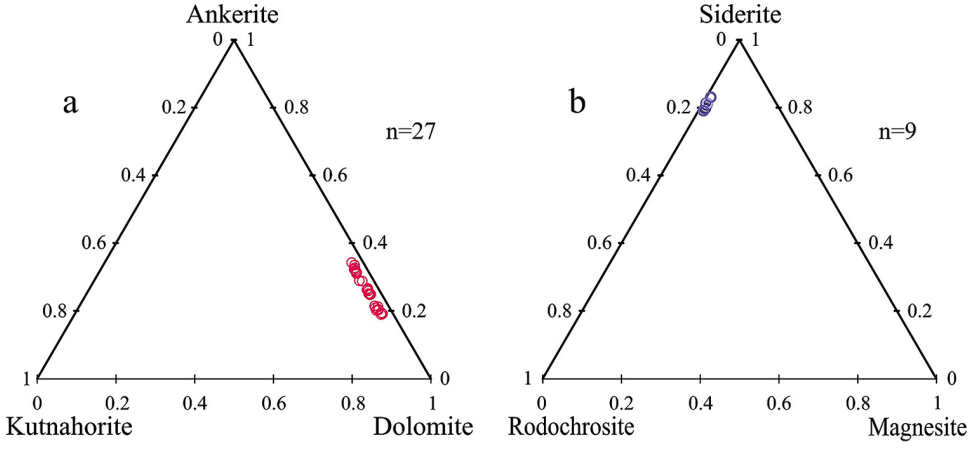

Fig. 14. a) Chemical composition of dolomite from Podlipa deposit dump samples in three-component system $CaMg(CO_3)_2$–$CaFe(CO_3)_2$–$CaMn(CO_3)_2$, in mol. %, n=27; **b)** chemical composition of siderite from Podlipa deposit dump samples in three-component system $MgCO_3$-$FeCO_3$-$MnCO_3$, in mol. %, n=9.

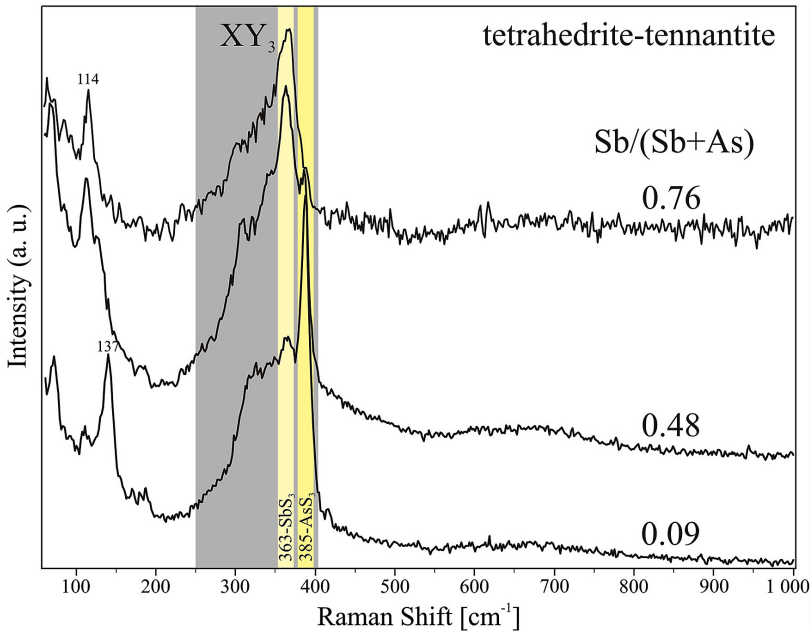

Fig. 15. Raman spectra of minerals of tetrahedrite-tennantite group. Shaded region represents vibrations of trigonal pyramids XY_3. Sb/(Sb+As) ratio reveals amount of substitution between Sb and As. Higher number (0.5-1.0) signifies tetrahedrite, lower one (0.0-0.5) tennantite. Complete chemical analyses are in the Tab. 1.

fractionation such as bacterial sulphate reduction, as it would result in much lighter sulphur spanning over a larger range (Hoefs, 2009). Regionally relevant sulphur isotope data are very scarce. Kantor (1975) measured sulphur isotope values of galena, chalcopyrite, and tennantite from strata-bound base-metal deposits Drienok and Farbište (10 and 5 km distance, respectively), emplaced in Anisian limestones of the Drienok Nappe, where he concluded that sulphur was delivered from a deep magmatic source related to previous acidic volcanism of Early Triassic age, modified by bacterial reduction. Genetic relation to our deposit is, however, excluded, due to much different tectonic setting as well as contrasting $\delta^{34}S$ pattern with large scatter from -14.89 to +14.69 ‰ and median at -4.79 ‰. The sulphur may have been remobilized from a deeper source, as the actual isotope values fit to general range of metamorphic rocks (Hoefs, 2009). Stable isotopes are a powerful tool in investigation of ore genesis; however, the scarcity of stable isotopes data hinders their use for regional correlations or tracking geochemical processes. Demand for this type of data appeals to increase existing body of information through publishing any reasonable isotope values.

6. CONCLUSIONS

Field, microscopic and mineralogical investigations at the Ľubietová – Podlipa Cu deposit shows that chalcopyrite is the dominant ore mineral in the dump samples, with less abundant tennantite and rare tetrahedrite. We have also described and characterized other rare primary minerals Bi-sulphosalt – kupčíkite, sulphoarsenides of Co and Ni – cobaltite-gersdorffite, a Ni-Co sulphide siegenite, and cassiterite.

Quartz is predominating among gangue minerals. Carbonates occur sporadically and mostly belong to the dolomite-ankerite series, with rare siderite and calcite. We consider siderite enriched in Mn as a potential source of manganese for the common supergene Mn-oxides at the Ľubietová-Podlipa deposit. Very rare cinnabar, silver or silver sulphides and native gold belong most likely to the cementation mineralization.

Raman microspectroscopy may be useful for discriminating between tetrahedrite-tennantite if small grain size or uneven surface do not allow for other means of identification. Raman shifts of certain peaks are diagnostic owing to the contrasting atomic mass of substituents (e.g., As *versus* Sb). In minerals of the dolomite group, Raman vibrational frequency of lattice modes decreases with increasing Fe concentration (i.e. mass of the cation). Substitution-dependent shifts in Raman wavenumbers imply a need for precaution when determining carbonates by Raman spectroscopy.

Mineralization at the Podlipa deposit originated in several stages. The early milky quartz was followed by carbonates with quartz and late dark quartz with sulphides. Individual stages were affected by tectonic activity and sulphide minerals show signs of recrystallization.

Acknowledgement: This study was financially supported by the VEGA grant No. 1/0538/15, by the APVV project 0663-10 and by the Operational Programme Research and Development through the projects: Centre of Excellence for Integrated Research of the Earth's Geosphere (ITMS: 26220120064) and Completion of technical infrastructure for research of geodynamical processes and global changes in Earth's history (ITMS: 26210120013), which had been co-financed through the European Regional Development Fund. V. Kollárová, P. Konečný and I. Holický are thanked for electron microprobe works and M. Chovan and J. Sejkora for the useful comments and suggestions that improved the text significantly.

References

András P., Lichý A., Križáni I., & Rusková J., 2009: The heavy metal sorption on clay minerals and risk of the AMD formation at the Reiner and Podlipa dump-fields at Ľubietová deposit (Slovakia). *Carpathian Journal of Earth and Environmental Sciences*, 4, 2, 133–146.

Bergfest A., 1951: Baníctvo v Ľubietovej na medenú rudu. [Mining for copper ore in Ľubietová]. Manuscript, Štátny ústredný banský archív, Banská Štiavnica, 89 p. [in Slovak]

Borishanskaya S.S, Vinogradova R.A. & Krutov G.A., 1981: Mineraly nikelya i kobal'ta (sistematika, opisanie i diagnostika). [Minerals of Nickel and Cobalt (Systematics, description and diagnostics)]. Izdatelstvo Moskovskogo Universiteta, Moscow, 216 p. [in Russian]

Breihaupt A., 1823: Vollständige Charakteristik des Mineral-Systems. Dresden, 267 p.

Burke E. A.J., 2001: Raman microspectrometry of fluid inclusions. *Lithos*, 55, 139–158.

Buzgar N. & Apopei A. I., 2009: The Raman study of certain carbonates. *Anatele Stiintifice Ale Universitatii A.I. Cuza din Iasi, Geologie*, 55, 2, 97–112.

Figuschová M., 1977: Sekundárne minerály medi z Ľubietovej. [Secondary minerals of copper from Ľubietová]. Collection of abstracts from the conference Ore forming processes in the Western Carpathians. Bratislava, 135–137. [in Slovak]

Frezzotti M. L., Tecce F., & Casagli A., 2012: Raman spectroscopy for fluid inclusion analysis. *Journal of Geochemical Exploration,* 112, 1–20.

Gunasekaran S., Anbalagan G. & Pandi S., 2006: Raman and infrared spectra of carbonates of calcite structure. *In:* Bellot-Gurlet L., Pages-Camagna S. & Coupry C. (Eds.): Raman Spectroscopy in Art and Archaeology II, *Journal of Raman Spectroscopy*, Special Issue, 37, 10, 892–899.

Hauerová J., Bláha M., Bartoň B., Linkešová M., Fodorová V., Makuša M., Pitoňák P. Spišiak J., 1989: Záverečná správa úlohy: Surovina: Cu (Sb, Ag, Ni, Co, Bi, W), vyhľadávací prieskum, I. podetapa. [The Ľubietová – Kolba deposit, Raw materials: Cu (Sb, Ag, Ni, Co, Bi, W), prospecting]. Manuscript, archive ŠGÚDŠ (Bratislava). [in Slovak]

Hem S.R & Makovicky E., 2004: The system Fe-Co-Ni-As-S. I. Phase relations in the (Fe,Co,Ni)$As_{0.5}S_{1.5}$ section at 650° and 500 °C. *The Canadian Mineralogist*, 42, 1, 43–62.

Hoefs J., 2009: Stable Isotope Geochemistry, 6th Edition. Springer-Verlag Berlin Heidelberg, 286 p.

Hvožďara P., 1971: Štúdium zlatých mineralizácií niektorých jadrových pohorí Západných Karpát. [Research of Au mineralizations in selected core mountain ranges in the West Carpathians]. Manuscript, archive ŠGUDŠ (Bratislava), 184 p. [in Slovak]

Hyršl J., 1991: Three polymorphs of $Cu_5(PO_4)_2(OH)$ from Ľubietová, Czechoslovakia. *Neues Jahrbuch für Mineralogie - Monatshefte*, 6, 281–287.

Ilavský J., Vozár J., Vozárová A. & Stankovič J., 1978: Komplexné zhodnotenie vrtov Lu-1, Lu-2, Lu-3 - Ľubietová. [Complex evaluation of bore holes: Lu-1, Lu-2, Lu-3, Ľubietová]. Manuscript, archive ŠGÚDŠ (Bratislava), 177 p. [in Slovak]

Jeleň S., Pršek J., Kovalenker V.A., Topa D., Sejkora J., Ozdín D. & Števko M., 2012: Bismuth sulphosalts of the cuprobismuthite, pavonite and aikinite series from the Rozália Mine, Hodruša-Hámre, Slovakia. *The Canadian Mineralogist*, 50, 2, 325–340.

Kantor J., 1975: Izotopy síry na Pb-Zn ložiskách z mezozoických karbonátov Západných Karpát. [Sulfur isotopes of the Pb-Zn deposits in Mesozoic carbonates of the Western Carpathians]. Manuscript, archive ŠGÚDŠ (Bratislava), 181 p. [in Slovak]

Kharbish Sh., Libowitzky E. & Beran A., 2007: The effect of As-Sb substitution in the Raman spectra of tetrahedrite-tennantite and pyrargyrite-proustite solid solutions. *European Journal of Mineralogy*, 19, 567–574.

Klemm D.D., 1965: Synthesen und Analysen in den Dreiecksdiagrammen FeAsS-CoAsS-NiAsS und FeS_2-CoS_2-NiS_2. *Neues Jahrbuch für Mineralogie – Abhandlungen*, 103, 205–255.

Koděra (Ed.), 1990: Topographical mineralogy of Slovakia, Volume 2. VEDA, Bratislava, 585–1098 p. [in Slovak with English preface and introduction]

Kravjanský I., 1956: Výročná správa o prieskume za rok 1955 na úseku Ľubietová – Cu. [Annual report of Cu exploration at Ľubietová area in 1955]. Manuscript, archive ŠGÚDŠ (Bratislava), 5 p. [in Slovak]

Láznička P., 1966: Kobaltin na ložisku Kolba východně od Ľubietové. [Cobaltite at the Kolba deposit eastern from Ľubietová]. *Časopis pro Mineralogii a Geologii*, 11, 177–180. [in Czech]

Lexa J., Bačo P., Hurai V., Chovan M., Koděra P., Petro M., Rojkovič I. & Tréger M., 2007: Explanatory notes to the metallogenetic map of Slovak Republic 1 : 500000. ŠGÚDŠ, Bratislava, 153 p. [in Slovak with English summary]

Li Y.B. & Liu J.M., 2006: Calculation of sulfur isotope fractionation in sulfides. *Geochimica et Cosmochimica Acta*, 70, 1789–1795.

Luptáková J., Milovská S., Biroň A., Jeleň S. & Andráš P., 2012: Study of secondary minerals of abandoned Cu deposit Ľubietová-Podlipa (Slovakia). *Acta Mineralogica-Petrographica*, *Abstract Series*, 7, 80.

Michňová J., 2009: Mineralogical and genetical study of primary hydrothermal mineralization at vicinity of Špania Dolina and Ľubietová. Manuscript, archive PriF UK, Bratislava, 214 p. [in Slovak with English abstract]

Michňová J., Ozdín D. & Bačík P., 2008: Fluid inclusion study and chemical composition of tourmaline from hydrothermal Cu-bearing deposit Ľubietová. *Bulletin mineralogicko-petrologického oddělení Národního muzea v Praze*, 16, 1, 100–108. [in Slovak with English abstract]

Mikuš T., Pršek J., Chovan M. & Makovický E., 2002: New type of hydrothermal mineralization in the Tatric tectonic unit (Western Carpathians): Ni-Bi-As mineral assemblage in the black shales. *In:* Michalík J., Šimon L. & Vozár J. (Eds.): Proceedings of the XVIIth Congress of CBGA, Bratislava, *Geologica Carpathica*, 53, Special Issue (CD).

Milovská S., Luptáková J., Biroň A. & Jeleň S., 2013: Mineralogy of Ľubietová - Podlipa deposit (The new data). *In:* Andráš, P. et al. (Eds.): Remnants of old mining activity at abandoned Cu-deposits. Ekomonitor, Chrudim, 165–87. [in Slovak with English abstract]

Moëlo Y., Makovický E., Mozgova N.N., Jambor J.L., Cook N., Pring A., Paar W., Nickel E.H., Graeser S., Karup-Møller S., Balic-Žunič T., Mumme W.G., Vurro F., Topa D., Bindi L., Bente K & Shimizu M., 2008: Sulfosalt systematics: a review. Report of the sulfosalt sub-committee of the IMA Commission on Ore Mineralogy. *European Journal of Mineralogy*, 20, 7–46.

Nakamoto K., 1997: Infrared and Raman spectra of inorganic and coordination compounds. Part A: Theory and applications in inorganic chemistry. Wiley-Interscience, 5th Edition, New York, 408 p.

Ozdín D., Sejkora J. & Račko M., 2016: Datovanie a paragenetická charakteristika hydrotermálnej mineralizácie v okolí Ľubietovej. [Dating and paragenetic characterization of hydrothermal mineralization in the vicinity of Ľubietová]. *In:* Proceedings of conference "Raw materials in the 21st century – Survey, research, exploitation, impacts", 6.-7. 10. 2016, Banská Štiavnica, pp. 42–43. [in Slovak]

Polák M. (Ed.), 2003: Outline of geological structure of the Starohorské vrchy Mts., Čierťaž Mts. and northern part of the Zvolenská kotlina Depression. ŠGÚDŠ, Bratislava, 218 p. [in Slovak with English summary]

Polák S., Filo I., Havrila M., Bezák V., Kohút M., Kováč P., Vozár J., Mello J., Maglay J., Elečko M., Olšavský M., Pristaš J., Siman P., Buček S., Hók J., Rakús M., Lexa J. & Šimon L., 2003: Geological map of the Starohorské vrchy Mts., Čiertaž Mts. and northern part of the Zvolenská kotlina Depression. ŠGÚDŠ, Bratislava.

Pršek J. & Mikuš T., 2006: Bi sulfosalts from the Ľubietová-Kolba occurrence. *Mineralia Slovaca*, 38, 2, 159–164. [in Slovak with English abstract]

Pršek J., Mikuš T., Makovický E. & Chovan M., 2005: Cuprobismutite, kupčíkite, hodrushite and associated sulphosalts from black shale hosted Ni-Bi-As mineralization at Čierna Lehota, Slovakia. *European Journal of Mineralogy*, 17, 155–162.

Řídkošil T. & Povondra P., 1982: The relation between posnjakite and langite. *Neues Jahrbuch für Mineralogie - Monatshefte*, 1, 16–28.

Řídkošil T., Šrein V., Fábry J., Hybler J. & Maximov B.A., 1992: Mrázekite $Bi_2Cu_3(OH)_2O_2(PO_4)_{2.2}H_2O$, a new mineral species, and its crystal structure. *Canadian Mineralogist*, 30, 1, 215–224.

Sejkora J., Števko M., & Macek I., 2013: Contribution to chemical composition of tetrahedrite from the Piesky copper deposit, the Špania Dolina ore district, central Slovakia. *Bulletin mineralogicko-petrologického Oddělení Národního Muzea* 21, 1, 89–103. [in Czech with English abstract]

Sejkora J., Števko M., Ozdín D., Pršek J. & Jeleň S., 2015: Unusual morphological forms of hodrušite from the Rozália vein, Hodruša-Hámre near Banská Štiavnica (Slovak Republic). *Journal of Geosciences*, 60, 11–22.

Slavkay M., Beňka J., Bezák V., Gargulák M., Hraško Ľ., Kováčik M., Petro M., Vozárová A., Hruškovič S., Knésl J., Knéslová A., Kusein M., Maťová V. & Tulis J., 2004: Mineral deposits of the Slovak Ore Mountains, Volume 2. ŠGÚDŠ, Bratislava, 286 p. [in Slovak with English summary]

Topa D., Makovicky E. & Balić-Žunić T., 2003: Crystal structures and crystal chemistry of members of the cuprobismutite homologue series of sulfosalts. *The Canadian Mineralogist*, 41, 6, 1481–1501.

Vlachovič J., 1964: Slovenská meď v 16. a 17. storočí. [Slovak copper in the 16th and 17th century]. SAV Bratislava, 327 p. [in Slovak]

Vozárová A. & Vozár J., 1988: Late Paleozoic in the Western Carpathians. ŠGÚDŠ, Bratislava, 314 p.

Zuberec J., Tréger M., Lexa J. & Baláž P., 2005: Mineral resources of Slovakia. ŠGÚDŠ, Bratislava, 350 p. [in Slovak with English summary]